공학석사학위논문

Development of the Snapshot Method for Six Degree-of-Freedom Flight Dynamics Simulation for a High Aspect Ratio Wing Aerial Vehicle

고세장비 날개를 가지는 항공기의 6 자유도 비행동역학 시뮬레이션을 위한 스냅샷 기법의 개발

2017 년 2 월

서울대학교 대학원

기계항공공학부

빈 영 빈

Abstract

Development of Snapshot Method for Six Degree-of-Freedom Flight Dynamics Simulation of a High Aspect Ratio Wing Aerial Vehicle

Young-been Been

Mechanical and Aerospace Engineering

The Graduate School

Seoul National University

In this thesis, a six degree-of-freedom flight simulation was developed considering the flexibility of an aircraft with high aspect ratio wings. A full three-dimensional finite element model of unmanned aerial vehicles was used. The object aircraft has main wings with aspect ratio over 20, and flight for long endurance in high altitude. To consider the flexibility of these aircraft, the present 'snapshot method' was developed that combines aerodynamic - structural dynamics - flight dynamics to analyze dynamic response. By applying this method, MATLAB/Simulink, which calculates the rigid body motion, and MSC.FlightLoads, which is responsible for aeroelastic trim analysis, were tightly linked into the present simulation framework.

Using the present simulation, aircraft response under various maneuver conditions was simulated. First, the trim analysis for the level cruise was performed. And the trim parameters, the stability derivative coefficients, and the moment of inertia were determined. Based on these results, the flight dynamics of the aircraft was

simulated according to the operation of the rudder and the aileron control surface. And the effect of the rigid and flexible body assumptions were confirmed. Also, these results were compared with the other existing simulation results based on the multibody dynamics under the same conditions. In order to predict the response of the aircraft under the gust, the simulation was performed by applying the two-dimensional 1-cosine discrete gust profile.

Keywords: High aspect ratio wing, Flight simulation, Flow field-structure-rigid body motion coupled analysis, Flight dynamics, Aeroelasticity, MATLAB/Simulink, MSC.FlightLoads

Student Number: 2015-20775

List of Contents

List of Figures

List of Tables

I. Introduction

1.1 Motivations

The roles of unmanned aerial vehicles(UAV) with fixed wings have become wider than ever. UAV's are widely used for communication relay, weather observation, disaster monitoring in civil area, as well as for reconnaissance, surveillance, attack missions in military area. In order to perform that mission effectively, long endurance in high altitude, and sometimes high agile maneuver are required. For these reasons, typical UAV's such as MQ-9 Reaper, X-HALE in USA, or Solar Impulse in Europe have high aspect ratio, flexible structure and light weight wings due to usage of composite materials [1]. This brings decrease in the integrity of structures although aerodynamic efficiency becomes improved. Therefore, when abrupt maneuver, gust, or disturbances are encountered, the flexible wings will experience large deflection, oscillations, even destruction [2]. As an example, Helios prototype fabricated in NASA crashed after in-flight breakage during the test flight in 2003. Unexpected flight paths may be induced and maneuver performance can be degraded [3, 4]. It will be beneficial if these problems can be taken into consideration from the design stage of aircraft development. In this thesis, a six degree-of-freedom flight simulation will be suggested as a countermeasure to such problem, while considering the structural flexibility of an aerial vehicle with high aspect ratio wings. If various maneuvers or the disturbance such as gusts are considered, it will be possible to reinforce structural design of the aircraft by analyzing accurately the loads acting on the

aircraft. Furthermore, analysis on the attitude changes or lift loss, which are additionally caused by the structural deformations of the aircraft, will also help to improve the performance of the flight control system. Such simulation will be useful in the design stages in order to save efforts in the design cycle and reduce the development cost.

1.2 Research Backgrounds

A study to analyze the effect of flexible structures in the flow field is defined as aeroelasticity and is shown in Figure 1.1. The left-hand side of the figure depicts static aeroelasticity by the relationship between external aerodynamic loads and internal elastic structural loads. In the equilibrium between both loads, the pressure distribution on the surface varies depending on the deformation state of the structure, and the load will be changed. If the structure is sufficiently flexible, such aeroelastic effect will become significant. This will influence the static stability of the structure and sometimes cause excessive deformation of the control surface, and thereby reduce or even reverse the intended control effect. If both loads are not in equilibrium, torsional divergence may occur and cause serious damage to the structure. The mechanical vibration shown in the lower side of the figure is mainly a phenomenon occurring in the structure, and the right-hand side of the figure is traditional flight dynamics. The interaction between aerodynamic and inertial forces causes translational and rotational rigid body movements. It is also affected by the static or

dynamic stability of the structure due to the external excitation force. The central part of the figure is about the phenomenon that occurs when three loads interact. Flutter is a self-induced periodic response in which the natural vibration mode of a structure is amplified by the frequency of external aerodynamic loads. Buffeting is the vibration of the structure due to the aerodynamic load fluctuations such as wakes and impacts separated from the aircraft in flight. It is also a representative dynamic response and stability phenomenon of the structure [5].

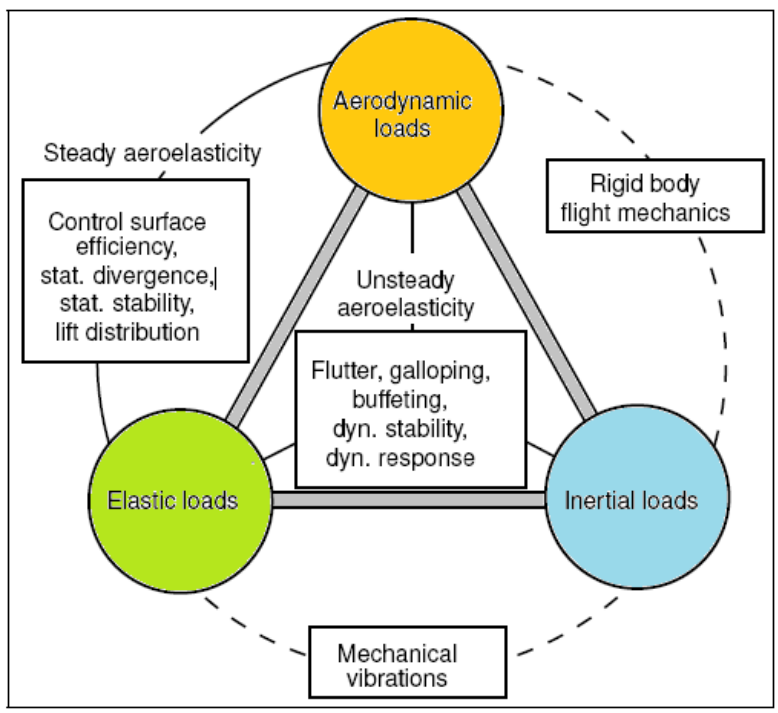

Figure 1.1 Collar's triangle diagram [5]

1.3 Previous Researches

Since the development of powered flight, interest in flight stability of aircraft such as torsional divergence and flutter has increased, and studies on flight mechanics, and aeroelasticity have begun [6, 7]. In 1911, Bryan introduced a fundamental concept of linear stability derivatives [8]. Until this time, however, the aircraft was regarded as a rigid body for its stability analysis. Since the advent of the jet engine, the flight speed of the aircraft has increased to the transonic regime. And the effect of aeroelasticity has become more significant by thin-walled wing structure with a sweep angle due to the compressible flow. Furthermore, large aircrafts with sufficient thrust have the decreased frequency ratio between the wing bending oscillation and aerodynamic rigid body mode like short period mode. As a result, efforts have been made to analyze the close relationship between aerodynamics and flight dynamics, mainly in the frequency domain and the Laplace domain. It was mainly focused on flight dynamics and the aeroelastic effect was excluded [9]. In 1955, frequency domain analysis procedures for aircraft subjected to gust loads was introduced by Bisplinghoff. But the flight test data were used instead of the aerodynamic load model [10, 11]. More accurate aerodynamic analysis, such as linearized potential theory, appeared in the 1970s. However, there were still limitations applied in the analysis of the frequency domain. Linear aerodynamic strip theory and equations of motion of the

elastic aircraft were coupled by Waszak et al. using Lagrangian mechanics [12]. They compared the frequency responses of the rigid aircraft, the two reduced-order models, and the full-order model, as shown in Figure 1.2.

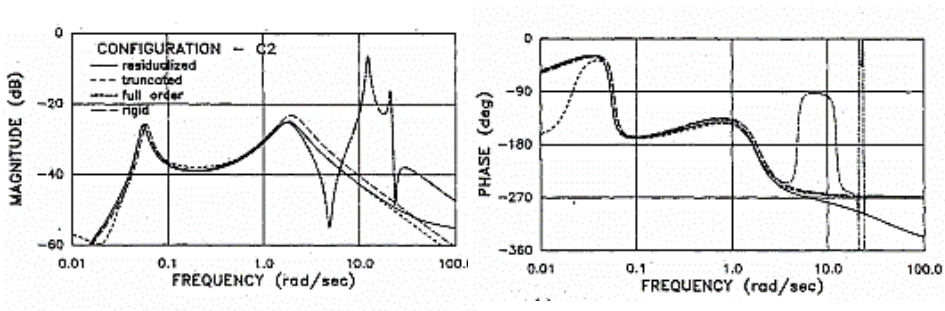

Figure 1.2 Frequency response analysis of three aircrafts model [12]

Drela completed flexible aircraft as an assemblage of non-linear structural beam formulation and solved unified algorithm by using a full Newtonian method for prediction of the flutter speed in frequency domain analysis, as shown in Figure 1.3. [13]. In his work, the aerodynamic model was a vortex/source lattice with wind-aligned trailing vorticity and Prandtl-Glauert compressibility correction.

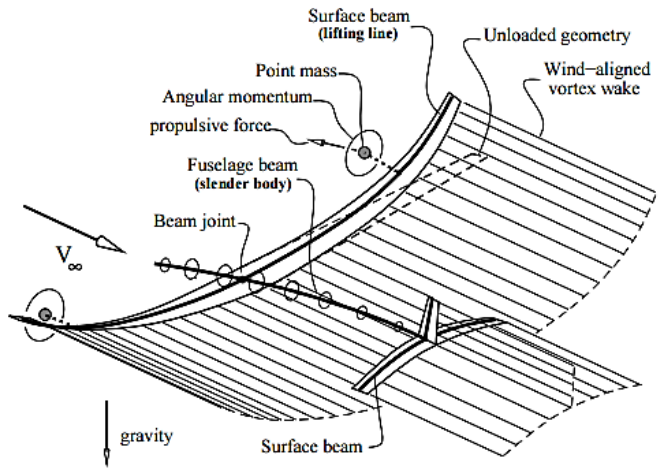

(a)

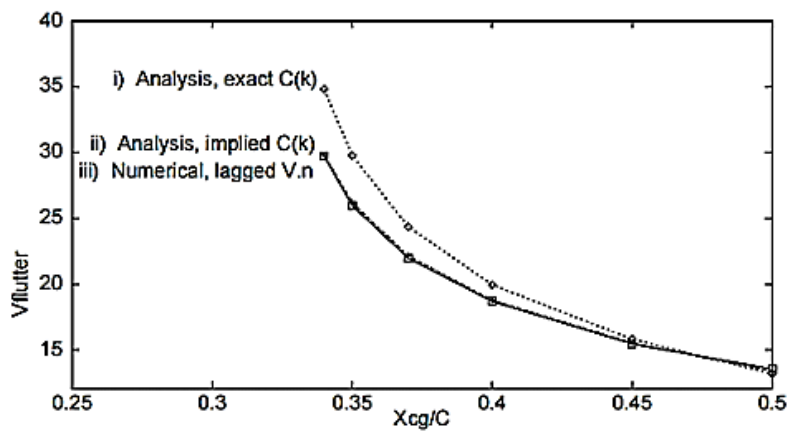

(b)

Figure 1.3 (a) Complete flexible aircraft as an assemblage of non-linear structural beam formulation, (b) the flutter speed in frequency domain analysis [13]

The coupled system in frequency domain is represented by a set of transfer functions. Its answer to external excitations, for instance by control inputs or by gusts, can readily be evaluated for a complete range of frequencies. However, such a transformation requires the linearization of the problem about a steady state and only allows small departures from this reference state to be considered. The unrestrained flight of an elastic aircraft is inherently non-linear including various aerodynamic phenomena, geometrical non-linearity in the case of large structural deformations, and non-linear terms in the rigid body laws of motion [14]. Therefore, in order to capture such non-linearity, the perception that time domain analysis is required has spread gradually. However, when compared with the analysis of frequency domain, this approach would be computationally more expensive. But in the early 21st century, computing power and speed have increased sufficiently to enable numerical analysis, including unsteady aerodynamic analysis, to be computed in the time domain. In addition, in 2001, Farhat et al. employed a solver of the time-dependent Euler equations of motion by using co-rotational finite element method for geometrically non-linear and unrestrained structural, geometrically conservative flow solver for CFD with moving fluid grids, and second-order time-accurate staggered algorithm for time-integrated coupling, as shown in Figure 1.4 [15].

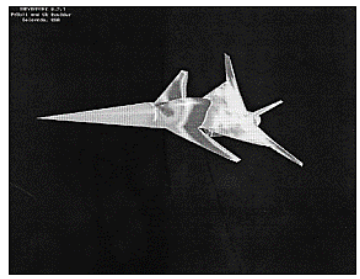

(a)

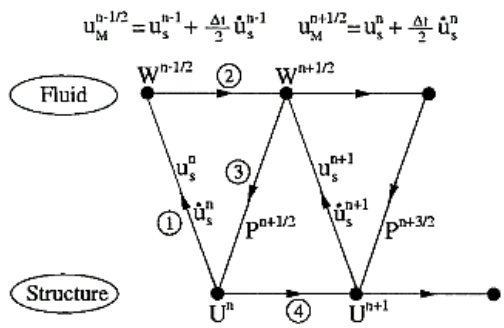

(b)

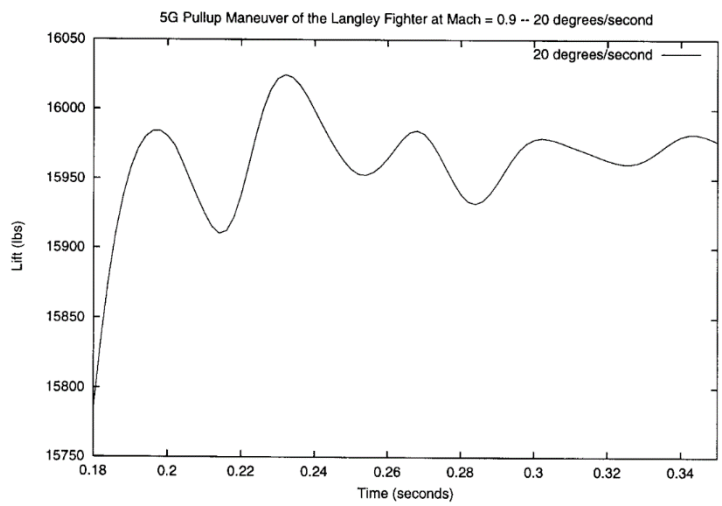

(c)

Figure 1.4 (a) Geometrically conservative flow solver for CFD, (b) second-order time-accurate staggered algorithm, (c) results of the time-dependent Euler equations of motion [15]

Then, Shearer et al. presented non-linear flight dynamic responses by using the coupled equations of the six degree-of-freedom rigid-body motions and the non-linear aeroelastic equations. They highlighted the importance of using the latter to properly analyze the very flexible vehicle motions, as shown in Figure 1.5 [3].

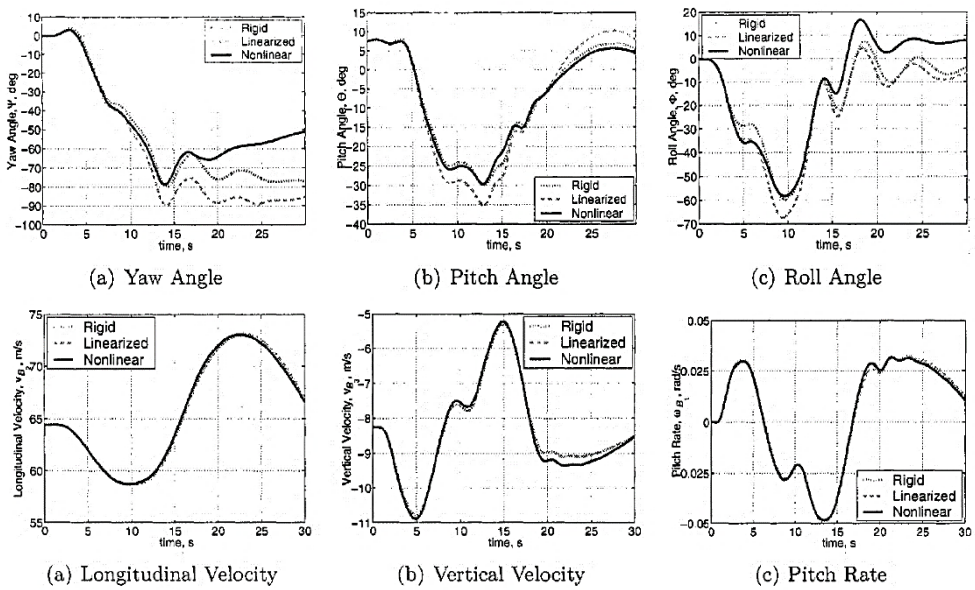

Figure 1.5 Three sets of solutions: rigid, linearized, and fully non-linear model [3]

Spieck et al. suggested a slightly different approach. The simulation of an aircraft in free flight was established by coupling the aerodynamic and the structural model of multi-body dynamics. Bi-directional interfaces transfer data between the multi-body dynamic system (MBS) with finite element model and CFD with algebraic aerodynamic force elements were time coupled by the conventional serial staggered

(CSS) method as shown in Figure 1.6 [17]. In addition, recently, there has been a simulation with the multi-body dynamics based on the principle of virtual work [5, 6] and the other one developed based on the floating frame of reference formulation [26].

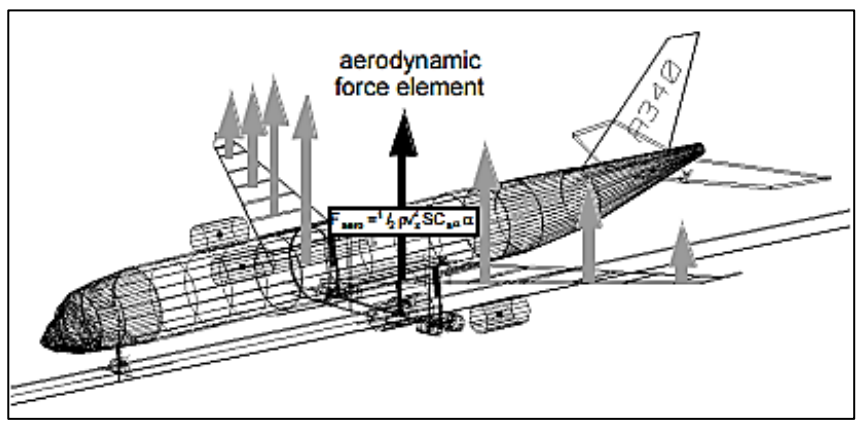

(a)

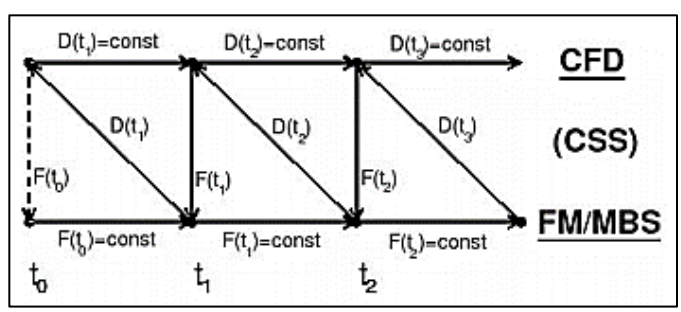

(b)

Figure 1.6 (a) Distributed aerodynamic force elements on MBS model, (b) time coupling scheme CSS [17]

1.4 Research Objectives and Thesis Outline

The final goal of this thesis is to develop a six degree-of-freedom simulation considering the structural flexibility of an aircraft. By using this simulation, flight state variation of an aircraft in either maneuver or gust will be predicted and the relevant transient loads will be estimated. Those loads will be used as an external force to analyze the structural dynamic response of the aircraft in the near future. At the present stage, the following goals are proposed to establish the framework of the simulation.

- **Aerodynamic – structural dynamic – flight dynamic coupling analysis**
- **Full three-dimensional finite element aircraft modeling**

A methodology for considering the structural flexibility of an aircraft in free flight is to capture the mutual interaction among the flow field, the structural deformation, and the rigid body motion as shown in Figure 1.7. First, due to the unique shape of the wing, there exists a pressure difference on the surface, which acts on the wing in the form of either lift or drag. This difference causes aerodynamic loads to distort the aircraft structure. In particular, the slenderer and the more flexible the wing becomes, the greater the amount of deformation will be. When the structure undergoes such a large deformation, the shape of the surface on which the air flows will be changed and the existing pressure distribution be changed further. This phenomenon will become

significant when the control system of an aircraft is operated and the control surface is deformed further. This pressure change will induce an aerodynamic load and affects the attitude and condition of the aircraft in flight. Also, when the attitude and speed of the aircraft changes, the state of the air that flows over the wing surface will also change. And the aerodynamic load will change further. When the attitude of an aircraft in flight changes, the inertial load acting on the structure will also change. This will cause additional deformation of the structure. In this way, the structural deformation of an aircraft in flight will affect the flow changes and rigid body motion, resulting in a change in the intended flight attitude and path. Therefore, the simulation in this thesis is planned to analyze the coupled aerodynamic - structural dynamics - flight dynamics in time domain. Although the relevant information is exchanged among each element of the analysis in a tight fashion, solvers which are responsible for the interpretation of each field will be employed independently. This modularized approach will become more complex but exhibit advantages compared with a set of unified formulas that obtain a simultaneous solution. It is possible to selectively combine the modularized solvers of each field according to the different flight conditions, as well as to upgrade to the analysis with the latest techniques. In particular, aerodynamic solvers are optimized for subsonic, transonic, and supersonic regimes. However, this coupled problems about explicit coupling and synchronization among all the fields need to be solved in order to combine the solvers adopted independently.

Structural analysis typically employs finite element models. Especially for time transient analysis, a fully linear formulation will be adopted. It is due to that modal analysis is applicable and the total deformation can be represented by the superposition of the structural eigenmodes [16]. However, such linearization will limit the deformation and displacement compared to the size of the structure in order to maintain validity of the method. Additional studies such as cross sectional analysis are required to create a reduced order model. Because of the improved computing capability achieved in recent years, this thesis employs the full three-dimensional modeling of an aircraft regarding structural dynamics. Therefore, since the structural analysis results can be directly derived, an additional work such as creating the reduced-order model or recovering the original model will not be required.

Finally, solvers in each field are implemented by adopting commercial analysis programs. When commercial analysis program is employed as a solver for each field, it will be easy to realize simulation framework. This is due to that it satisfies the purpose of modularization and there is no need to develop each solver directly. Therefore, additional effort to validate the solver may be reduced, and practicality and versatility are increased.

In Chapter 2, as described above, system design and implementation strategies for six degree-of-freedom flight simulation framework will be presented. The background information for the solvers that are responsible for each individual fields will then be

described. Finally, the communication scheme of commercial analysis programs will be described by coupling each solver considering actual implementation. Chapters 3 will discuss various application for the validation of the simulation, and Chapter 4 will present summary and research plan for the future.

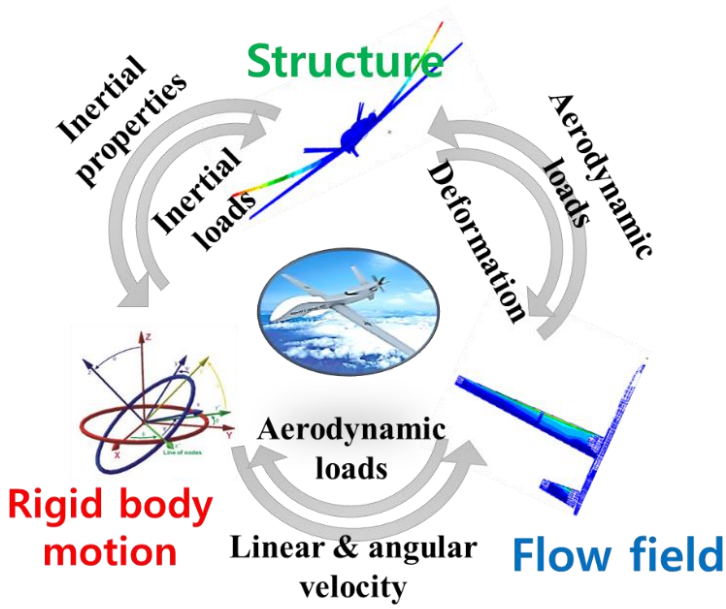

Figure 1.7 Scheme of the mutual interaction among the flow field, the structural deformation and the rigid body motion [14]

II. Theoretical Background

In this chapter, a strategy of implementing a six degree-of-freedom flight simulation for a flexible aircraft is introduced. This thesis introduces the formalization of analytical models employed in the three solvers and explains the process of communicating the information that those exchange. Finally, the framework is established by a combination of commercial analysis programs.

2.1 Snapshot Method

To build the modularized approach of aerodynamic-structure-rigid body motion described in Chapters 1-4, the solver responsible for each field will be called sequentially. In addition, in order to analyze it in terms of time, synchronization of each single field will be required within a short time interval especially when a snapshot photograph is taken. The shorter the time step among these synchronizations is, the more accurate the combined solution scheme will become. But when the computation becomes more complex, its efficiency will need to be considered. Therefore, choice of a particular time domain coupling methodology will be important. As shown in Figure 2.1, the flight dynamics solver imports the moment of inertia information of the deformed aircraft obtained in the previous step from the structural analysis solver, and the aerodynamic influence coefficients from the aerodynamic

solver. Then, during a short time step, the rigid body motion equation will be solved to derive the attitude change and flight path of the aircraft, and provide the environmental change information to the aerodynamic solver. The aerodynamic solver determines the aerodynamic load based on the shape information of the deformed aircraft predicted in the previous time step and provides it to the structural analysis solver. Finally, the structural analysis solver will determine the deformation of the aircraft structure based on the attitude information from the flight dynamics solver. The resulting solution is modified by relaxation factor ω as shown in Eq. (2.1).

$$U_{i+1} = \omega U_{i+1}^{'} + (1 - \omega)U_i \tag{2.1}$$

In this equation, U_i is the result of the predictor step for each field derived from the computation for 1→2→3 as shown in Figure 2.1. $U_{i+1}^{'}$, as a result of the corrector step predicted from 4→5→6 in the same condition, converges to U_{i+1}, which is the result of the next step due to the relaxation factor.

This coupling iterations only represent instances of information exchange among the fields during the convergence towards the steady state. This new method will be named as 'snapshot method.' In the following chapters, the coupled formulation of each solver responsible for aerodynamic analysis, structural analysis, and flight dynamics will be introduced.

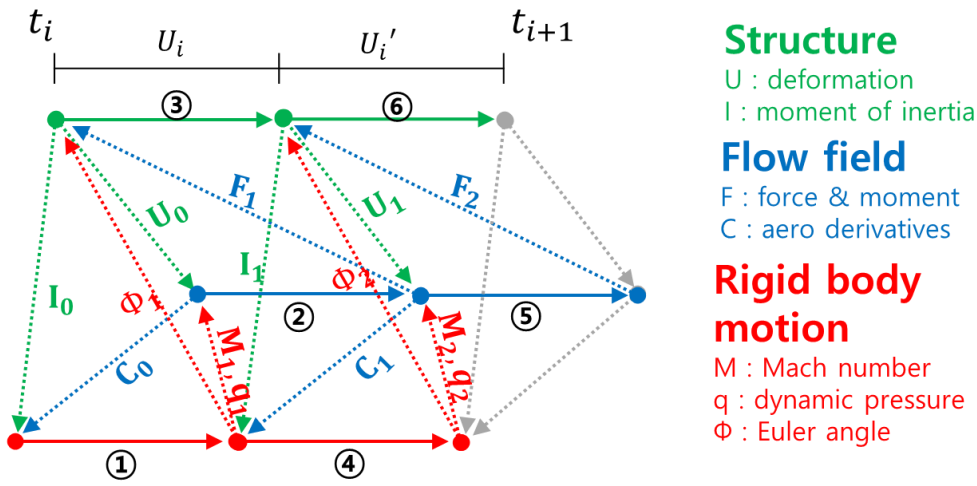

Figure 2.1 Quasi-steady temporal coupling scheme for the snap-shot method

2.2 Flight Dynamics Solver

2.2.1 Rigid Body Motion

Flight dynamics solver, the main component of the present simulation that predicts the dynamic response of the free-flying aircraft, analyzes the equations of rigid body motion. Its relevant derivations are based on Blakelock [18]. The equations of motion are derived by applying Newton's laws of motion, which relate the summation of the external forces and moments to the linear and angular accelerations of the system. To derive the equation, following assumptions will be made and an axis system be defined. First, the body axis lies in the aircraft and J_{xy} and J_{yz} are equal to zero. At this time, the exact direction of *X*-axis is not specified from the origin, but in general it is not along a principal axis. Second, the weight of the aircraft remains constant during any particular dynamic analysis. Third, the aircraft body is assumed to be a rigid body. Thus, any two points on or within the airframe will remain fixed with respect to each other. Fourth, unless otherwise stated the atmosphere is fixed with respect to the inertial frame of reference.

2.2.2 Wind Axis Coordinate System

By definition the wind axes are oriented so that the X wind axis X_W may lie along the total velocity vector V_T of the aircraft. The wind axes are then oriented with respect to the body axes through the angle of attack α and the

sideslip angle β as shown in Figure 2.2. The relation between the components of velocity in body axis and the total velocity vector is shown in Eq. (2.2). P, Q, and R are the components of the angular velocity are roll, pitch, yaw rate in body axis, respectively.

$$U = V_T \cos\beta \cos\alpha$$

$$V = V_T \sin\beta \tag{2.2}$$

$$W = V_T \cos\beta \sin\alpha$$

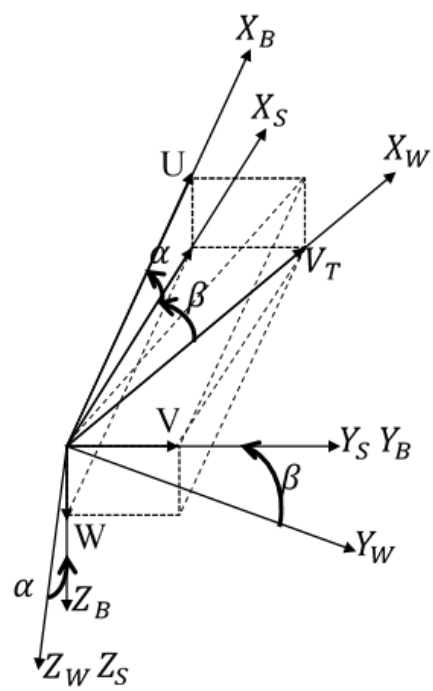

Figure 2.2 Transformation of the velocity vector V_T from the wind to body axes

2.2.3 Formulation of Wind Axis Equation of Motion

The wind axis equations of rigid body motion are derived from the body axis equation of motion shown in Eq. (2.3).

$$\sum \Delta F_x = m(\dot{U} + WQ - VR)$$

$$\sum \Delta F_y = m(\dot{V} + UR - WP) \tag{2.2}$$

$$\sum \Delta F_z = m(\dot{W} + VP - UQ)$$

Dividing Eq. (2.3) by the mass yields the body axis accelerations

$$A_{XB} = \dot{U} + WQ - VR$$

$$A_{YB} = \dot{V} + UR - WP \tag{2.3}$$

$$A_{ZB} = \dot{W} + VP - UQ$$

where these are the accelerations resulting from the aerodynamic and gravitational forces acting on the aircraft. By differentiating Eq. (2.2).

$$\dot{U} = \dot{V_T} c \cos\beta \cos\alpha - V_T \dot{\beta} \sin\beta \cos\alpha - V_T \dot{\alpha} \cos\beta \sin\alpha$$

$$\dot{V} = \dot{V_T} \sin\beta + V_T \dot{\beta} \cos\beta \tag{2.4}$$

$$\dot{W} = \dot{V_T} c \cos\beta \sin\alpha - V_T \dot{\beta} \sin\beta \sin\alpha + V_T \dot{\alpha} \cos\beta \cos\alpha$$

Substituting Eqs. (2.2) and (2.4) into Eq. (2.3),

$$A_{XB} = \dot{V}_T c \cos\beta \cos\alpha - V_T \dot{\beta} \sin\beta \cos\alpha - V_T \dot{\alpha} \cos\beta \sin\alpha$$

$$+V_T \cos\beta \sin\alpha\, Q - V_T \sin\beta\, R$$

$$A_{YB} = \dot{V}_T \sin\beta + V_T \dot{\beta} \cos\beta + V_T \cos\beta \cos\alpha\, R - V_T \cos\beta \sin\alpha\, P \qquad (2.5)$$

$$A_{ZB} = \dot{V}_T c \cos\beta \sin\alpha - V_T \dot{\beta} \sin\beta \sin\alpha + V_T \dot{\alpha} \cos\beta \cos\alpha$$

$$+V_T \sin\beta\, P - V_T \cos\beta \cos\alpha\, Q$$

Transforming the body axis accelerations into stability axes as shown in Figure 2.3 (a),

$$A_{XS} = A_{XB} \cos\alpha + A_{ZB} sin\alpha$$

$$A_{YS} = A_{YB} \qquad (2.6)$$

$$A_{ZS} = -A_{XB} \sin\alpha + A_{ZB} \cos\alpha$$

Transforming the stability axis accelerations into wind axes as shown in Figure 2.3 (b),

$$A_{XW} = A_{XS} \cos\beta + A_{YS} sin\beta$$

$$A_{YW} = -A_{XS} \sin\beta + A_{YS} \cos\beta \qquad (2.7)$$

$$A_{ZW} = A_{ZS}$$

Substituting Eq. (2.6) into Eq. (2.7),

$$A_{XW} = (A_{XB} \cos\alpha + A_{ZB} sin\alpha) \cos\beta + A_{YB} sin\beta$$

$$A_{YW} = -(A_{XB} \cos\alpha + A_{ZB} sin\alpha) \sin\beta + A_{YB} \cos\beta \qquad (2.8)$$

$$A_{ZW} = -A_{XB}\sin\alpha + A_{ZB}\cos\alpha$$

Substituting Eq. (2.5) into Eq. (2.8) and solving the equations for $\dot{V}_T$, $\dot{\alpha}$, and $\dot{\beta}$ respectively yields

$$\begin{aligned} \dot{V}_T &= A_{XW} \\ \dot{\alpha} &= \frac{A_{ZW}}{V_T\cos\beta} + Q - (R\sin\alpha + P\cos\alpha)\frac{\sin\beta}{\cos\beta} \\ \dot{\beta} &= \frac{A_{YW}}{V_T} - (R\cos\alpha - P\sin\alpha) \end{aligned} \tag{2.9}$$

But from Figure 2.3 (c)

$$\begin{aligned} R_S &= R\cos\alpha - P\sin\alpha \\ P_S &= R\sin\alpha + P\cos\alpha \end{aligned} \tag{2.10}$$

Substituting Eq. (2.10) into Eq. (2.9),

$$\begin{aligned} \dot{V}_T &= A_{XW} \\ \dot{\alpha} &= \frac{A_{ZW}}{V_T\cos\beta} + Q - P_S\frac{\sin\beta}{\cos\beta} \\ \dot{\beta} &= \frac{A_{YW}}{V_T} - R_S \end{aligned} \tag{2.11}$$

These are the wind axis equations for the rigid body motion. The wind axis accelerations in Eq. (2.11) are given by Eq. (2.7), where the stability axis accelerations are

$$A_{XS} = \left(\frac{T}{m} + g_x\right)\cos\alpha + g_z sin\alpha - \frac{qSC_D}{m}$$

$$A_{YS} = g_y + \frac{qSC_Y}{m} \tag{2.12}$$

$$A_{ZS} = -\left(\frac{T}{m} + g_x\right)\sin\alpha + g_z\cos\alpha - \frac{qSC_L}{m}$$

where is the engine thrust in pounds, assumed to be along X_B. C_D, C_Y, and C_L are the total drag, side force, and lift coefficients respectively, and g_x, g_y, and g_z are the components of gravity.

The typical definition of the stability derivatives in the restrained longitudinal aircraft may be illustrated by the lift coefficient noted by $C_L = -C_Z$ [19].:

$$C_Z = -C_L = C_{Z_0} + C_{Z_\alpha}\alpha + C_{Z_{\delta_e}}\delta_e + C_{Z_q}\frac{q\bar{c}}{2V} + C_{Z_{\dot{\alpha}}}\frac{\dot{\alpha}\bar{c}}{2V} + C_{Z_{\ddot{z}}}\frac{\ddot{z}}{g} + C_{Z_{\ddot{\theta}}}\frac{\ddot{\theta}\bar{c}}{2g}$$

0 0 0

Only the lift coefficient is described here, and the other coefficients are summarized in the block 1 in Figure 2.5.

To transform the components of the angular velocity of the aircraft from the earth axis to the aircraft fixed axis system as shown in Figure 2.4, the components $\dot{\Psi}$, $\dot{\Theta}$, and $\dot{\Phi}$ will be projected along the OX, OY, and OZ axes to obtain

$$P = \dot{\Phi} - \dot{\Psi}\sin\Theta$$

$$Q = \dot{\Theta}\cos\Phi + \dot{\Psi}\cos\Theta\sin\Phi \tag{2.13}$$

$$R = -\dot{\Theta}\sin\Phi + \dot{\Psi}\cos\Theta\cos\Phi$$

These equations can be solved for $\dot{\Psi}$, $\dot{\Theta}$, and $\dot{\Phi}$ to yield

$$\dot{\Psi} = \frac{(R\cos\Phi + Q\sin\Phi)}{\cos\Theta}$$

$$\dot{\Theta} = Q\cos\Phi - R\sin\Phi \tag{2.13}$$

$$\dot{\Phi} = P + \dot{\Psi}\sin\Theta$$

Euler angles are estimated by substituting angular rates obtained from rotational equations of motion into Eq. (2.13).

Figure 2.5 shows the block diagram of the flight dynamics consisting of the wind and body axis system, formulated equations of rigid body motion, and aerodynamic force and moment coefficients described above [20].

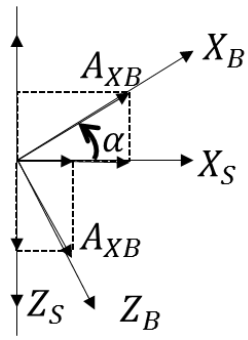

(a)

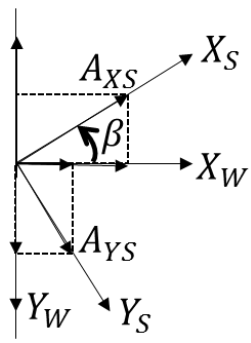

(b)

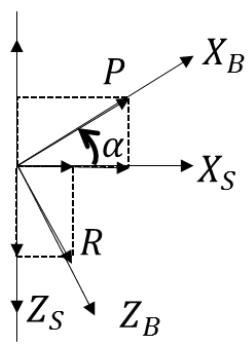

(c)

Figure 2.3 (a) Transformation of the body axes acceleration to stability axes, (b) Transformation of stability axes acceleration to wind axes, (c) Stability axes roll and yaw rates

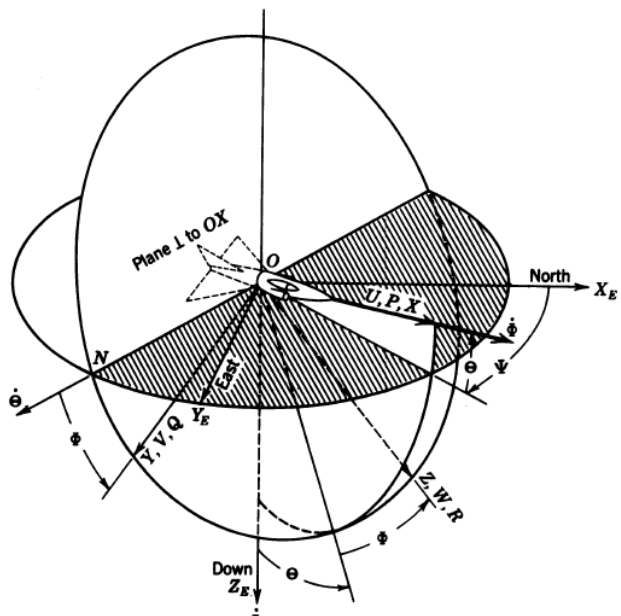

Figure 2.4 Sketch of Euler angles and aircraft fixed axes [18]

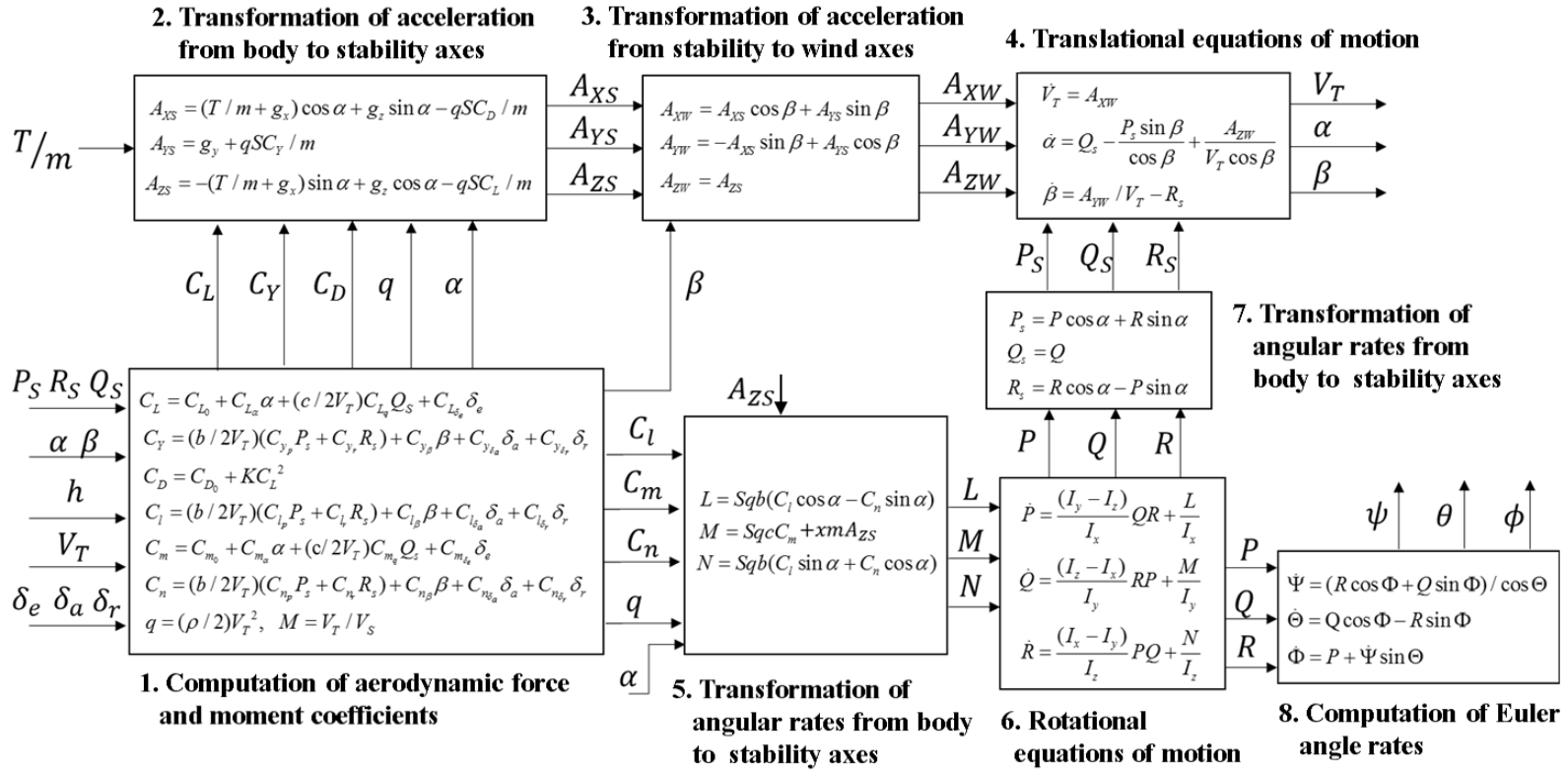

Figure 2.5 Block diagram of wind axis system and flight dynamics for 6-DOF simulation [20]

2.2.4 Implementation by using MATLAB/Simulink

MATLAB/Simulink, developed by MathWorks, is a graphical programming environment as functional mock-up interface for modeling, simulating and analyzing multi-domain dynamic systems. It offers tight integration with the rest of the MATLAB environment and can either drive MATLAB or be scripted from it. Simulink is widely used in automatic control and digital signal processing for multi-domain simulation and model-based design. This program provides a convenient aerospace block-set library and primary interface in a graphical block diagramming tool. The block diagram of the flight dynamics described in the previous section was constructed as a numerical program using the functional blocks of this library. The resulting program is illustrated in Figure 2.5 and can perform dynamic response analysis of the aircraft for continuous time history.

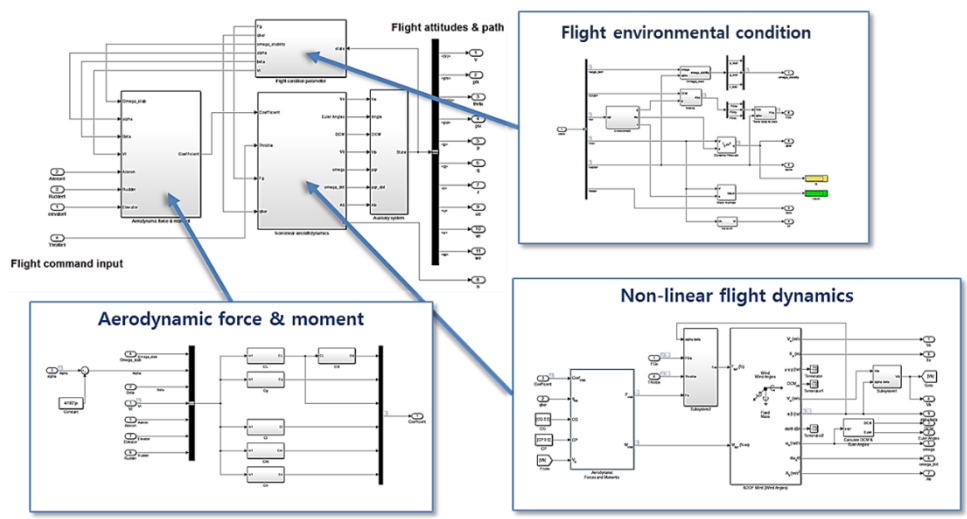

Figure 2.6 Rigid body motion solver and subsystem arrangement plan

In order to execute this program, specific information of the aircraft such as configuration, weight, moment of inertia, etc. and aerodynamic influence coefficients are additionally required. Then, after defining the flight environment to be simulated, results in determining the flight attitude and path of the aircraft can be obtained by continuously prescribing the control command signal. The detailed items are summarized in Table 2.1.

Table 2.1 Input information for MATLAB/Simulink program

Aircraft specification	**Initial flight condition**	**Aerodynamic stability derivatives**		
Length	Angle of attack	C_{L_0}	C_{L_α}	C_{L_q}
Wing span	Angle of sideslip	$C_{L_{\delta e}}$	C_{m_0}	C_{m_α}
Wing area	Altitude	C_{m_q}	$C_{m_{\delta e}}$	C_{y_p}
Chord	Euler angle	C_{y_r}	C_{y_β}	$C_{y_{\delta a}}$
Incidence angle	Angular rate	$C_{y_{\delta r}}$	C_{l_β}	C_{l_p}
Center of pressure	True air speed	C_{l_r}	$C_{l_{\delta a}}$	$C_{l_{\delta r}}$
Weight	Location	C_{n_β}	C_{n_p}	C_{n_r}
Center of gravity	Control command signals	$C_{n_{\delta a}}$	$C_{n_{\delta r}}$	C_{D_0}

2.3 Aerodynamics Solver

2.3.1 Aerodynamic Finite Element Model for Flow Field

In this thesis, a full three – dimensional aerodynamic finite element model was employed as an aerodynamics solver. The aerodynamic elements are strips, boxes, or segments of bodies that are combined to idealize the aircraft for the computation of aerodynamic forces. These elements, like structural elements, are defined by their geometry and their motions are defined by degrees of freedom at aerodynamic grid points. Requirements of the aerodynamic theory often dictate the geometry of the boxes. For example, the doublet-lattice methods assume trapezoidal boxes with their edges parallel to the free-stream [21]. A panel model consisting of boxes with this method was adopted in this thesis. Aerodynamic calculations are performed using a Cartesian coordinate system. By the usual convention, the flow is in the positive x-direction, and the x-axis of every internal aerodynamic element must be parallel to the flow in its undeformed location. This corresponds to an assumption of aerodynamic small disturbance theory, further simplification of the potential theory. The structural coordinate systems may be defined independently, since the use of the same system for both may place an undesirable restriction upon the description of the structural model. All aerodynamic element and grid point information are transformed to the aerodynamic coordinate system. The aerodynamic grid points are physically located at the centers of the boxes for the lifting surface theories.

2.3.1 Doublet Lattice Subsonic Lifting Surface Theory

The theoretical basis of the doublet-lattice method applied to the boxes among the elements of the internal aerodynamic model is the linearized aerodynamic potential theory and an extension of the steady vortex-lattice method to unsteady flow. The undisturbed flow is uniform and is either steady or gusty harmonically. Each of the interfering surface panels is divided into small trapezoidal lifting element boxes such that the boxes can be arranged in strips parallel to the free stream with surface edges, fold lines, and hinge lines lying on box boundaries. The unknown lifting pressures are assumed to be concentrated uniformly across the one-quarter chord line of each box. There is one control point per the 75% chordwise station and spanwise center of the box, and the surface downwash boundary condition is satisfied at each of these points.

2.3.2 Formulation of the Doublet Lattice Method

Formulation of the method is as follows. Details of the explanations regarding the derivations are included in Ref. 21. Three matrix equations summarize the relationships required to define a set of aerodynamic influence coefficients [22]. Those are the basic relationships between the lifting pressure and the dimensionless vertical or normal velocity induced by the inclination of the surface to the airstream. In the expressions, w_j is the downwash, f_j is pressure on lifting element j, $\bar{q}$ is

flight dynamic pressure, and $A_{jj}(M,k)$ is aerodynamic influence coefficient matrix, a function of Mach number, and reduced frequency.

$$\{w_j\} = [A_{jj}]\{\frac{f_j}{\bar{q}}\} \tag{2.14}$$

It is the substantial differentiation matrix of the deflections to obtain downwash, where w_j^g is static aerodynamic downwash; it includes, primarily, the static incidence distribution that may arise from an initial angle of attack, camber, or twist, k is reduced frequency, and ${D_{jk}}^1$, ${D_{jk}}^2$ are real and imaginary parts of substantial differentiation matrix, respectively.

$$\{w_j\} = [{D_{jk}}^1 + ik{D_{jk}}^2]\ \{u_k\} + \{w_j^g\} \tag{2.15}$$

Integration of the pressure is done to obtain forces and moments, where u_k, P_k are displacements and forces at aerodynamic grid points, and S_{kj} is integration matrix.

$$\{P_k\} = [S_{kj}]\{f_j\} \tag{2.16}$$

The aerodynamic stiffness matrix relates the aerodynamic loads to the displacements, where $Q_{kk}(M,k)$ is the aerodynamic influence coefficient matrix.

$$\{P_k\} = \bar{q}\,[Q_{kk}]\{u_k\} \tag{2.17}$$

This matrix is computed from the three matrices of Eqs. (2.14), (2.15), and (2.16).

$$\{Q_{kk}\} = [S_{kj}]\,[A_{jj}]^{-1}[{D_{jk}}^1 + ik{D_{jk}}^2] \tag{2.18}$$

The doublet lattice method compute the S_{kj}, A_{jj}, and D_{jk} matrices at user-supplied Mach numbers and reduced frequencies. Then, matrix decomposition and forward and backward substitution are used in the computation of the Q_{kk} matrix.

2.4 Structure Dynamics Solver

2.4.1 Linear Static Analysis using the Finite Element Model

The structural dynamics solver performs a linear static structural analysis on the model using the finite element method. The structural model applied in this thesis also reflects the full three-dimensional configuration of the aircraft with a wing aspect ratio of 20 and is generated using MSC.PATRAN. Among the structural features of the aircraft, the laminated structures mainly were modeled by CQUAD4 elements and the rest CBAR, CROD, CBEAM, HEXA, TRIA3. Composite material includes each lamination layer properties, but non-linearity of the properties was not considered.

2.5 Coupling of Aerodynamic and Structural Dynamics Solver

2.5.1 Interconnection of the Structural Analysis with Aerodynamic Model

For coupling aerodynamics and structural dynamics solver, structural and aerodynamic grids need to be connected by interpolation. The interpolation method is called spline. The theory involves the mathematical analysis of beams and plates. Aeroelastic problems are solved using the structural degrees of freedom, enforcing those to be independent degrees of freedom. The aerodynamic degrees of freedom are dependent. A matrix is derived that relates the dependent degrees of freedom to the independent ones. The structural degrees of freedom may include certain grid components. The interpolation from the structural deflections to the aerodynamic deflections and the relationship between the aerodynamic forces and the structurally equivalent forces act on the structural grid points as shown in Figure 2.7.

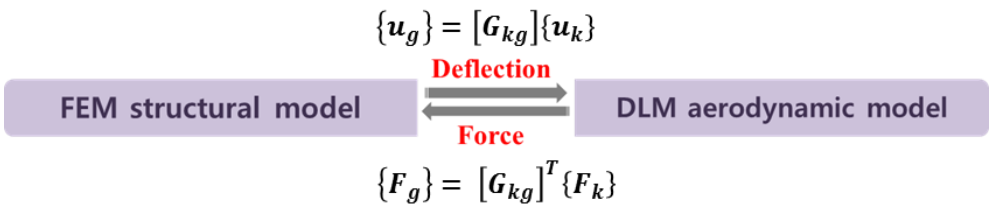

Figure 2.7 Coupling between the aerodynamic and the structural solver by using splining methods

2.5.2 Formulation of the Spline Method

Formulation of the method is as follows. Details of the explanations regarding derivations are included in Ref. 21. The spline method leads to an interpolation matrix G_{kg} that relates the components of structural grid point displacements u_g to those of the aerodynamic grid points u_k,

$$\{u_k\} = [G_{kg}]\{u_g\} \tag{2.19}$$

The aerodynamic forces F_k and their structurally equivalent values F_g acting on the structural grid points therefore do the same virtual work in their respective deflection modes,

$$\{\delta u_k\}^T\{F_k\} = \{\delta u_g\}^T\{F_g\} \tag{2.20}$$

where δu_k and δu_g are virtual deflections. Substituting Eq. (2.19) into the left-hand side of Eq. (2.20) and rearranging yields

$$\{\delta u_g\}^T([G_{kg}]^T\{F_k\} - \{F_g\}) = 0 \tag{2.21}$$

from which the required force transformation is obtained because of the arbitrariness of the virtual deflections.

$$\{F_g\} = [G_{kg}]^T\{F_k\} \tag{2.22}$$

Eqs. (2.19) and (2.22) are both required to complete the formulation of aeroelastic problems in which the aerodynamic and structural grids do not coincide, that is, to interconnect the aerodynamic and structural grid points. The transpose of the deflection interpolation matrix is all that is required to connect the aerodynamic forces to the structure.

2.5.3 Quasi-steady Aeroelastic Analysis

Quasi-steady aeroelastic problems deal with the interaction of aerodynamic and structural forces on a flexible vehicle that results in a redistribution of the aerodynamic loading as a function of airspeed. It considers application of the steady-state aerodynamic forces to a flexible aircraft, which deflects under the applied loads resulting in perturbed aerodynamic forces. The solution of these problems assumes that the system comes to a state of quasi-static equilibrium. The aerodynamic load redistribution and consequent internal structural load and stress redistributions are important output to the structural solver. Also, the aerodynamic load redistribution

and consequent modifications to aerodynamic stability and control derivatives are important output to the aerodynamic solver.

2.5.4 Formulation of Aeroelastic Trim Analysis

Formulation of the analysis is as follows. The following explanations have been adapted from Ref. 21. For quasi-steady aeroelastic trim analysis, the aerodynamic forces are transferred to the structure using the spline matrix in Eqs. (2.19) and (2.22) reduced to the *a*-set to form an aerodynamic influence coefficient matrix Q_{aa}, which provides the forces at the structural grid points due to structural deformations,

$$[Q_{aa}] = [G_{ka}]^T [W_{kk}][S_{kj}][A_{jj}]^{-1}[D_{jk}][G_{ka}] \tag{2.23}$$

and the second matrix Q_{ax}, which provides forces at the structural grid points due to unit deflections of the aerodynamic extra points,

$$[Q_{ax}] = [G_{ka}]^T [W_{kk}][S_{kj}][A_{jj}]^{-1}[D_{jx}] \tag{2.24}$$

The complete equations of motion in the *a*-set degrees of freedom require structural stiffness matrix K_{aa}, structural mass matrix M_{aa}, and vector of applied loads P_a for example, mechanical, thermal, and gravity loads plus aerodynamic terms due to user input pressures or downwash velocities. The a-set equations will become as follows,

$$[K_{aa} - \bar{q}[Q_{aa}]]\{u_a\} + [M_{aa}]\{\ddot{u}_a\} = \bar{q}[Q_{ax}]\{u_x\} + \{P_a\} \tag{2.25}$$

This is the basic set of equations used for static aeroelastic analysis. In the general case, rigid body motions are included in the equations to represent the free-flight characteristic of an aircraft.

The objective of the quasi-steady aeroelastic analysis is to determine the loads on the aircraft due to a quasi-static maneuver. The maneuver is described by a set of trim parameters. The subset of the trim parameters is defined by the user and the remaining trim parameters are determined during the analysis. In the analysis all the loads are assumed to be constant in time. The elastic loads can only be constant in time if the elastic deformations are constant in time. The total deformation can be split into the elastic deformation u_a^e and the rigid body motion u_a^r,

$$\{u_a\} = \{u_a^e\} + \{u_a^r\} \tag{2.26}$$

Then $\ddot{u}_a = \ddot{u}_a^r$ and a rigid body motion usually does not induce damping forces. The rigid body motion can be written as superposition of the rigid body modes. The modes are determined from the *r*-set degree of freedom defined on the support point. At this point the implementation of aeroelastic analysis introduces a mathematical technique that is based on the inertial relief analysis without aeroelastic effects.

$$D_{ar} = \begin{bmatrix} -K_{ll}^{-1}K_{lr} \\ I_{rr} \end{bmatrix} \tag{2.27}$$

It is known as the rigid body mode matrix. And it can be shown that it is only a function of the geometry of the object aircraft, where I_{rr} is the r-dimensional unit matrix. The undetermined accelerations can be directly specified using two relations. The first relation will be obtained from the assumption of quasi-steady equilibrium. It specifies that

$$\{\ddot{u}_a\} = \{\ddot{u}_a^r\} = [D_{ar}]\{\ddot{u}_r\} \tag{2.28}$$

where $\ddot{u}_r$ are the rigid body structural accelerations in global reference frame. The second relation states that $\ddot{u}_r$ is related to a subset of trim parameters on aerodynamic extra points u_x via

$$\{\ddot{u}_r\} = [T_{rR}][\mathrm{T}_{Rx}]\{u_x\} \tag{2.29}$$

where u_x consists of the rigid body accelerations in the body-fixed reference frame, the aerodynamic attitudes, the rotational rates, and the control surface deflections.

$$u_x = \{\ddot{u}_R \ \alpha \ \beta \ \frac{\mathrm{pb}}{2\mathrm{V}} \ \frac{q\bar{c}}{2V} \ \frac{rb}{2V} \ \delta_c\} \tag{2.30}$$

In addition, T_{Rx} is the Boolean matrix that selects accelerations from the aerodynamic extra points and T_{rR} is a matrix that transforms accelerations from the aerodynamic reference point to the supported degrees of freedom. This second matrix is a function of only the geometry of the object aircraft.

Therefore, the basic trim equation of linear quasi-steady aeroelasticity reads

$$\left[K_{aa} - \bar{q}[Q_{aa}]\right]\{u_a^e\} = \{P_a\} + \overline{(q}[Q_{ax}] - [M_{aa}][D_{ar}][T_{rR}][\mathrm{T}_{Rx}])\{u_x\} \quad (2.31)$$

The external loads P_a and the subset of the trim parameters u_x are given. The problem is to determine the remaining trim parameters and the elastic deformation u_a^e. Subsequently, the loads on the aircraft can be determined. First, the basics of the trim analysis are explained considering the rigid aircraft and next, the effect of the flexibility of the aircraft is studied. The elastic deformations are linearly independent of the rigid body modes and relative to the body-fixed reference frame.

If trim parameters do depend on time, the trim equation is solved for each discrete point in time. These momentary trim formulations are quasi-steady approximations of the original dynamic problems. The number of free trim parameters may exceed the number of *r*-set degrees of freedom. In this case, the free trim parameters are determined such that the trim equation is satisfied, and the sum of the squares of the trim variables is minimized.

In addition, the aerodynamic stability derivatives are the derivatives of the non-dimensional aerodynamic load resultants with respect to the trim parameters and refer to the body-fixed reference frame [23]. Stability derivatives are derived from the resultants of the aerodynamic loads given by

$$\mathrm{A}_R = [T_{rR}]^T[D_{ar}]^T[A_a](u_a^e, u_x) \quad (2.32)$$

The non-dimensional aerodynamic load resultants are defined by

$$\mathrm{C}_R = \frac{NA_R}{\bar{q}} \tag{2.33}$$

where normalization matrix N is consist of reference area S, span width b, and chord length $\bar{c}$.

$$N = \frac{1}{S}\begin{bmatrix} 1 & & & & & & \\ & 1 & & & & & \\ & & 1 & & & & \\ & & & 1/b & & & \\ & & & & 1/\bar{c} & & \\ & & & & & 1/b & \end{bmatrix} \tag{2.34}$$

The resultants with respect to the trim parameters generally

$$\frac{\partial \mathrm{C}_R}{\partial u_x} = \frac{[\mathrm{N}]}{\bar{q}}\left(\frac{\partial \mathrm{A}_R}{\partial u_x} + \frac{\partial \mathrm{A}_R}{\partial u_a^e}\frac{\partial u_a^e}{\partial u_x}\right) \tag{2.35}$$

In a rigid body aircraft,

$$\frac{\partial \mathrm{C}_R}{\partial u_x} = [\mathrm{N}][T_{rR}]^T[D_{ar}]^T[Q_{ax}] \tag{2.36}$$

In a restrained flexible aircraft,

$$\frac{\partial \mathrm{C}_R}{\partial u_x} = [\mathrm{N}][T_{rR}]^T[D_{ar}]^T([Q_{ax}] + [Q_{al}][U_{lx}^r]) \tag{2.36}$$

2.5.5 Implementation by using MSC.FlightLoads

MSC.FlightLoads is the commercial program consisting of pre- and post-processor MSC.PATRAN and MSC.NASTRAN. As an open architecture environment for aeroelastic analysis, this system will be useful as a convenient tool for model

development and creation by the venue for critical loads computation and management with GUI for MSC. NASTRAN. MSC. PATRAN can be used to generate an aerodynamic model that reflects the configuration of the three-dimensional finite element structural model of the aircraft to be analyzed [24]. Based on the formulations described above, MSC.FlightLoads performs aeroelastic analysis on coupled structures and aerodynamics. It provides responses that take into account the flexibility of each component or complete fuselage in time domain. Figure 2.8 is a conceptual diagram showing the system architecture of MSC.FlightLoads [25]. The required input information of MSC.FlightLoads is a three-dimensional finite element structural analysis including mass and stiffness as described above, and a three-dimensional aerodynamic analysis considering the configuration and performance of the control surface. Based on the results of the trim analysis at the desired flight conditions and conditions, aerodynamic stability derivatives can be derived from the aerodynamic analysis, while taking into account the aerodynamic stability and control characteristics of the aircraft. Also, the load acting on each component from the structural model and the displacement, the moment of inertia of the deformed shape can be predicted.

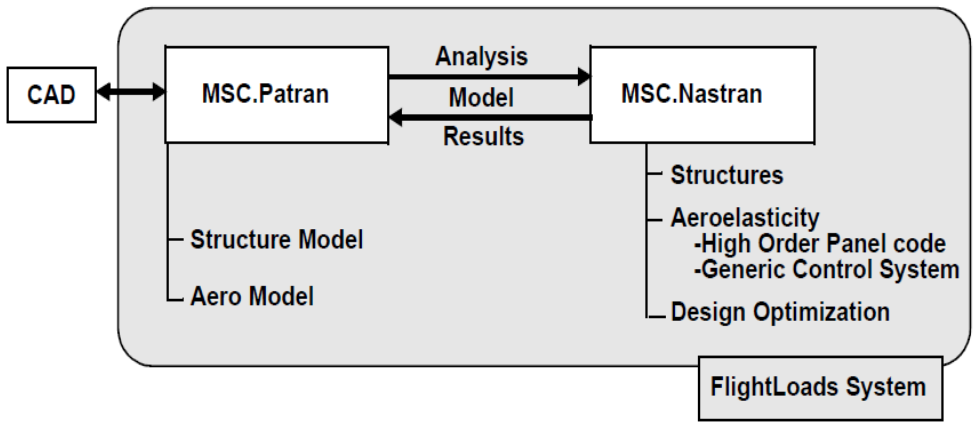

Figure 2.8 Conceptual diagram of the system architecture of MSC.FlightLoads

2.6 Coupled Aerodynamic, Structure, and Flight Dynamics Solver

2.6.1 Aeroelastic and Rigid Body Motion Coupled Analysis

This section introduces the way how to couple aerodynamic-structural dynamics-flight dynamics solvers. First, the method of coupling aerodynamics and structural dynamics is to perform aeroelastic analysis. Quasi-steady trim analysis is conducted by using the coupled flow field and structural model. The resulting information is then provided to the flight dynamics analysis of the rigid aircraft. At this time, it can be broadly divided into two parts as shown in Figure 2.9. First, the information of aerodynamic performance derived from aerodynamic analysis as a result of aeroelastic analysis is needed for the flight dynamics analysis of rigid aircraft. The information of the flight state and the environment derived from the flight dynamics analysis of the

rigid aircraft is provided to the aerodynamic analysis. Next, distribution of the structural loads has to be modified by considering distribution of the inertial loads, which are equivalent to the external loads generated by the rigid aircraft linear and angular acceleration. For this reason, the inertial properties of the aircraft derived from the structural model is provided to the structural dynamics analysis. In order to derive this information from aeroelastic analysis, the flight attitude information can be provided from the flight dynamics of the rigid aircraft.

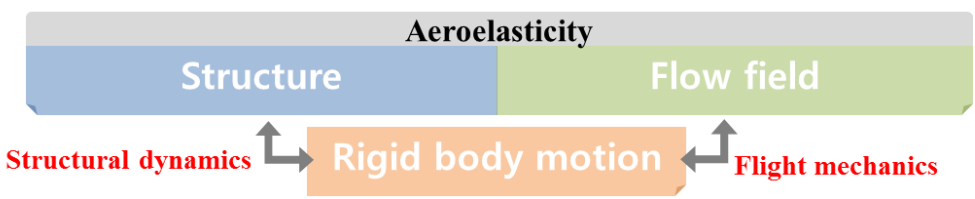

Figure 2.9 Coupling between the rigid aircraft and the aeroelasticity

2.6.2 Implementation of Simulation Framework

In order to implement the simulation analysis described above, the communication scheme is established as shown in Figure 2.10 using a commercial program that is responsible for the solver of each field. First, the full three-dimensional finite element

structure model and the doublet lattice aerodynamic model of the aircraft are supplied into MSC.FlightLoads, and the deformation of structural and aerodynamic model are obtained by aeroelastic trim analysis. The deformed structural and aerodynamic configuration is fed back into the program for analysis for the next time step. At this time, the aeroelastic trim analysis requires information of the flight state like control surface deflection, flight attitude of aircraft, and environments like Mach number, dynamic pressure. This information can be obtained by MATLAB/Simulink program by analyzing rigid body motion based on flight dynamics. For this analysis, the aerodynamic stability derivatives and inertial moment reflecting the aircraft geometry can be provided by MSC.FlightLoads. At the same time, control command signals are required in MATLAB/Simulink program. By repeating this procedure for the total analysis duration, six degree-of-freedom flight simulation can be implemented considering the structural flexibility of the aircraft.

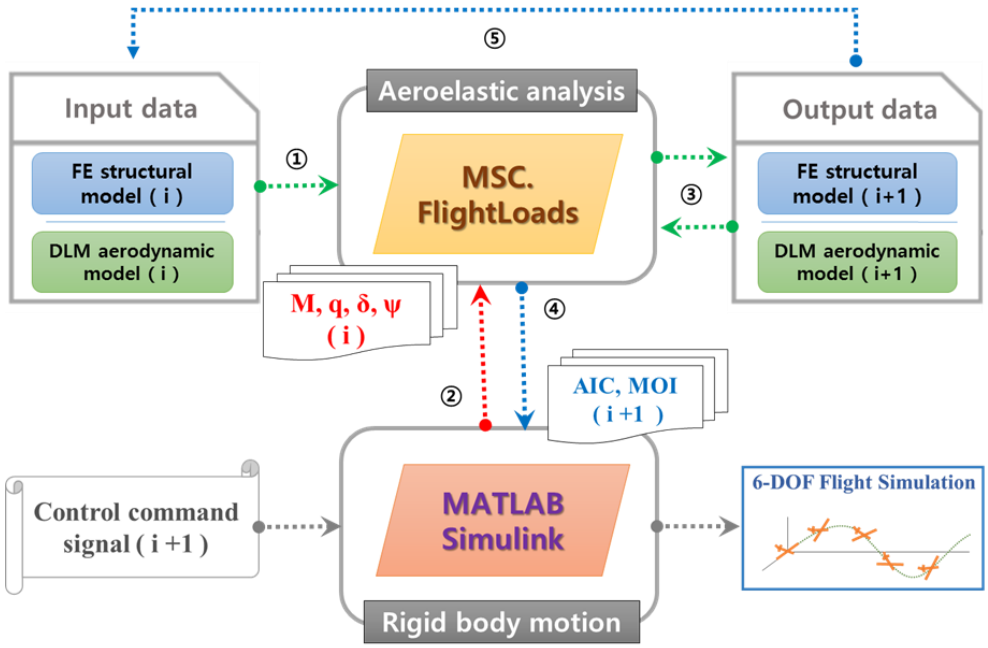

Figure 2.10 Flow chart of the communication scheme for the present simulation framework

III. Numerical Results

3.1 Flight Simulation for Maneuver

3.1.1 Trim Analysis and Simulation Results for Level Cruise

In this thesis, the aircraft used for the simulation was a UAV that has main wings with aspect ratio over 20, and mainly flight for long endurance in high altitude. The specific configuration and information of the UAV are shown in Figure 2.6. The trim analysis was performed using MSC.FlightLoads to derive the aerodynamic stability derivatives and inertial moment information required for the simulation for various maneuver conditions. First, the trim analysis for the level cruise was carried out at the main mission operating speed of 75 m/s and the main mission altitude of 10,000 m. Table 3.1 summarizes the parameters required for the trim analysis of level cruise.

Table 3.2 summarizes the results of the trim analysis and compared with the trim analysis results of the multibody dynamics-based simulation (MBS) performed on the previous research under the same conditions in Kim et al. [26]. The values of all the parameters in the rigid aircraft assumption were consistent for both simulations. In the flexible body assumption, however, the value of angle of attack showed 0.6% difference, the difference in elevator deflection was 2.3%, and that in elevator deflection was 10%. It was concluded that these discrepancies were mainly caused by very different approaches of both simulations. Table 3.3 are the aerodynamic stability

derivatives and moment of inertia information derived from MSC.FlightLoads while performing the trim analysis considering the flexibility of the aircraft.

By the aerodynamic-structure coupled analysis on the trim, the deformation of the flexible aircraft was compared with rigid one as shown in Figure 3.2. It was confirmed that the deformation amount of the tip of the wing is approximately 0.5 m. Figure 3.3 shows the distribution of aeroelastic loads acting on the aircraft. The upper figure shows the nodal rigid component, and the lower one shows the nodal elastic component. These results can be derived at every time step during the simulation by applying the snapshot method. In addition, the results such as the stress distribution can be extracted at every grid point of the three-dimensional finite element structure model of the UAV.

Based on the above information, simulation was performed using MATLAB/ Simulink. At the altitude of 10,000 m and the speed of 75 m/s, the flight duration was 10 seconds and the flexibility of the aircraft was included. Figures 3.4 shows the flight paths and attitudes as simulation results for a level cruise. During the total flight duration, the flight distance was 750 m and the flight path and attitude of the aircraft remained almost constant. The discrepancy of the initial trim value between the rigid and flexible aircraft was maintained until the end. Verification was confirmed that the results of the multibody dynamics simulation when the same condition was used and object aircraft was similar.

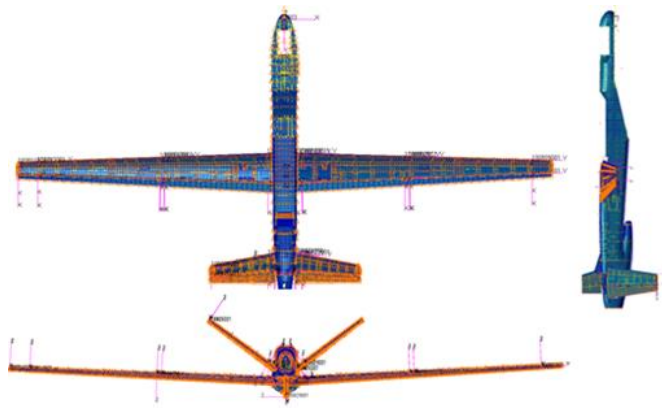

(a)

Nodes	30,619
Elements	56,187
Coordinate Frames	32
Material Properties	81
Element Properties	2,229

(b)

Figure 3.1 (a) Configuration of the target aircraft, (b) Specific information of the finite element model [18]

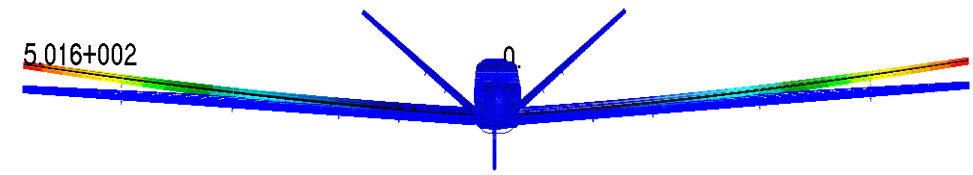

Figure 3.2 Comparison of deformation between the rigid and flexible aircraft assumption

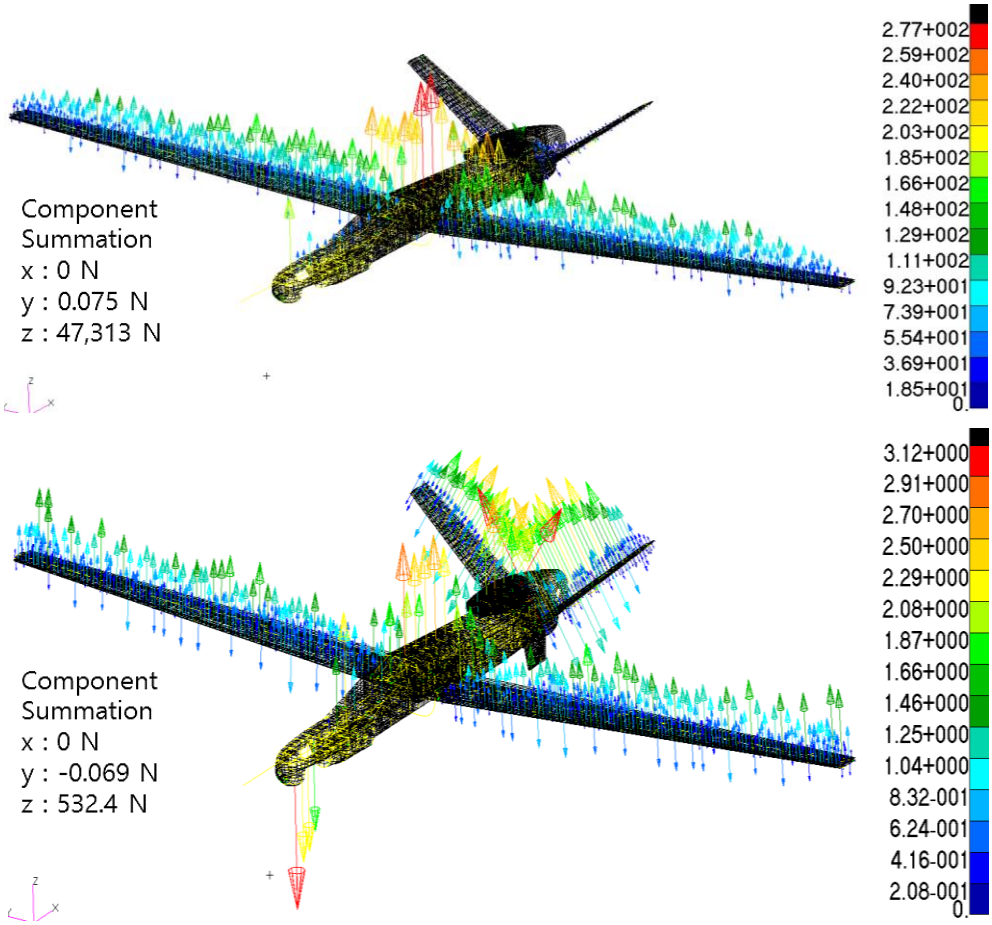

Figure 3.3 Aeroelastic loads on the aircraft

(upper: nodal rigid component, lower: nodal elastic component)

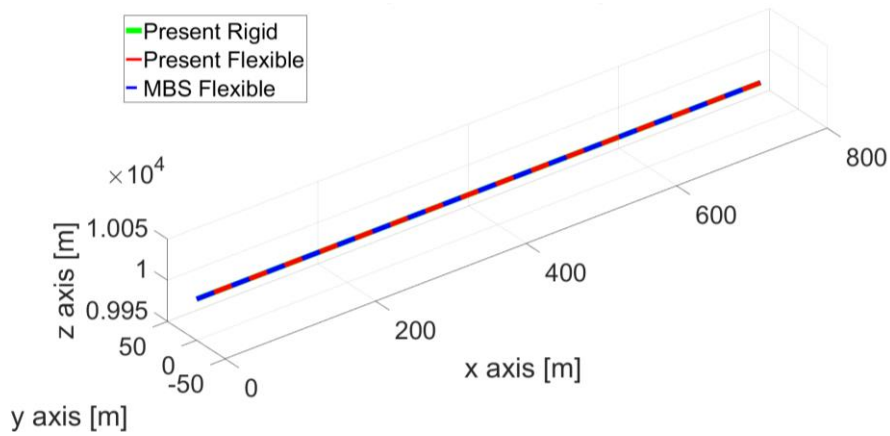

(a) flight path

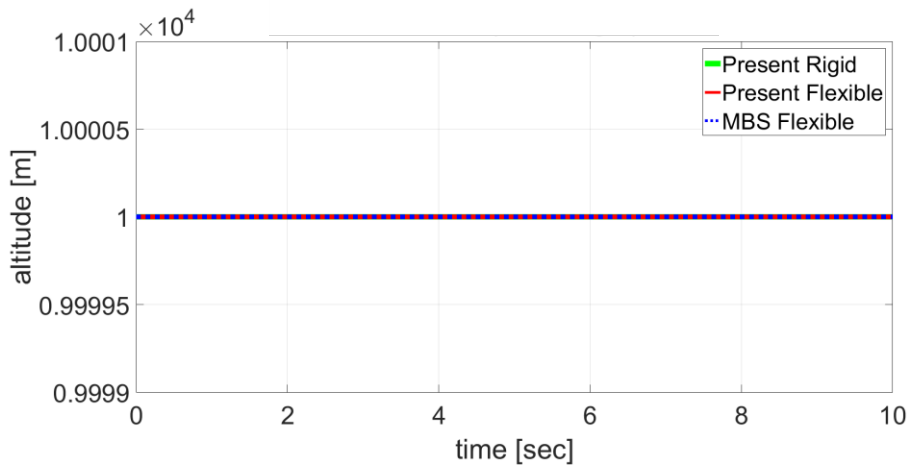

(b) altitude

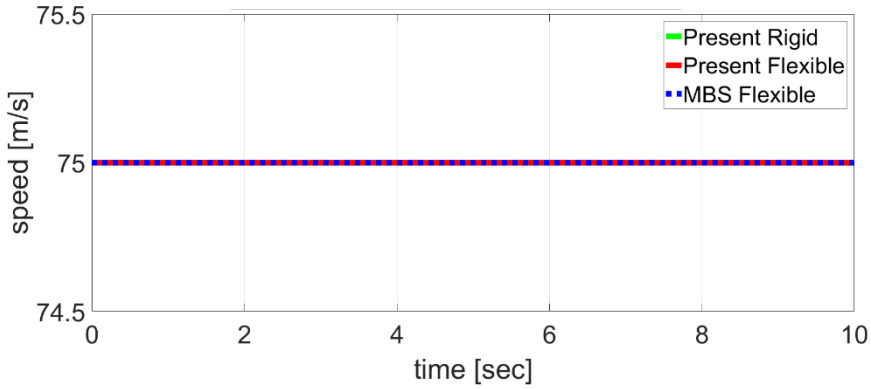

(c) true air speed

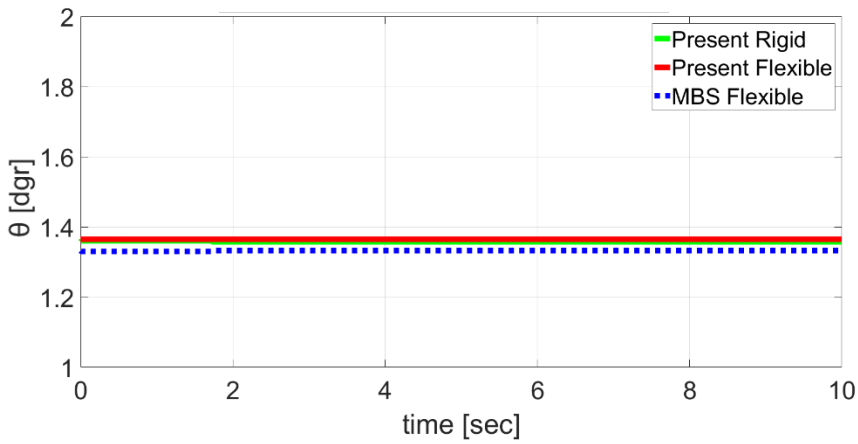

(d) Euler angle

Figure 3.4 Comparison of the level cruise simulation

Table 3.1 Input information of MSC.FlightLoads for trim analysis in level cruise

Trim parameters		Level cruise
Control surfaces	Aileron	0
	Flap	0
	Rudder	0
	Elevator	Free
Attitudes	Pitch	0
	Roll	Free
	Yaw	Free
Condition	Altitude	10,000 m
	True air speed	75 m/s
	AOA	Free
	AOS	Free
	y-axis Linear acc.	0
	z-axis Linear acc.	-1
	x-axis Angular acc.	0
	y-axis Angular acc.	0
	z-axis Angular acc.	0

Table 3.2 Comparison with the trim analysis results of present and MBD simulation

Trim parameters		AOA[°]	AOS[°]	Roll[°]	Yaw[°]	Elevator[°]	Thrust[N]
Rigid	Present	5.357	0	0	0	-1.82	4904
	MBS	5.357	0	0	0	-1.82	4904
Flexible	Present	5.365	0	0	0	-1.71	4457
	MBS	5.332	0	0	0	-1.67	4901
Difference [%]		0.6	0	0	0	2.3	10

Table 3.3 Aerodynamic stability derivatives and moments of inertia in the result of MSC.FlightLoads

Altitude: 10,000 m True air speed: 75 m/s Level cruise Flexible body					
Aerodynamic Stability Derivatives					
C_{L_0}	7.1456× 10^{-1}	C_{y_β}	-3.5112× 10^{-1}	$C_{l_{\delta a}}$	-4.1966× 10^{-1}
C_{L_α}	6.2127× 10^{0}	C_{y_p}	-1.3400× 10^{-1}	$C_{l_{\delta r}}$	-4.9630× 10^{-2}
C_{L_q}	1.1185× 10^{1}	C_{y_r}	1.3431× 10^{-1}	C_{n_β}	2.6270× 10^{-2}
$C_{L_{\delta e}}$	6.2860× 10^{-1}	$C_{y_{\delta a}}$	-5.9200× 10^{-2}	C_{n_p}	5.5012× 10^{-3}
C_{m_0}	-3.8090× 10^{-2}	$C_{y_{\delta r}}$	-3.5623× 10^{-1}	C_{n_r}	-2.6780× 10^{-2}
C_{m_α}	-1.4087× 10^{0}	C_{l_β}	-9.0330× 10^{-2}	$C_{n_{\delta a}}$	-1.6001× 10^{-4}
C_{m_q}	-1.9856× 10^{1}	C_{l_p}	-6.9517× 10^{-1}	$C_{n_{\delta r}}$	6.4420× 10^{-2}
$C_{m_{\delta e}}$	-1.9171× 10^{0}	C_{l_r}	1.7480× 10^{-2}	K	7.3699× 10^{-2}
Moments of Inertia [kg × m^2]					
I_{xx}	3.4788× 10^{4}	I_{yx}	-1.3635× 10^{2}	I_{zx}	5.5984× 10^{2}
I_{xy}	-1.3635× 10^{2}	I_{yy}	3.9883× 10^{4}	I_{zy}	2.5447× 10^{0}
I_{xz}	5.5984× 10^{2}	I_{yz}	2.5447× 10^{0}	I_{zz}	7.3538× 10^{4}

3.1.2 Simulation Results of Response to Elevator Control Input

Simulation was performed to confirm the response of the elevator to the control signal input. At the altitude of 10,000 m and the speed of 75 m/s, the total analysis duration was 10 seconds. During that duration, the elevator control signal was prescribed by adding (-) 0.5 ° to the trim value in the level cruise. This was to examine the longitudinal flight of the aircraft, and the thrust was maintained to be the trim value of the level cruise. The snapshot method was applied to the simulation to consider the flexibility of the aircraft.

Figure 3.5 shows results of the simulation about flight path, flight state in terms of the speed, and Euler angle as the attitude. The altitude of the aircraft was increased by an average of 21 m and the flight distance decreased by 20 m compared to the level cruise. There was a discrepancy between the rigid and flexible aircraft assumption. And the discrepancy was also confirmed in the results of the multibody dynamics simulation, but the overall tendency was maintained.

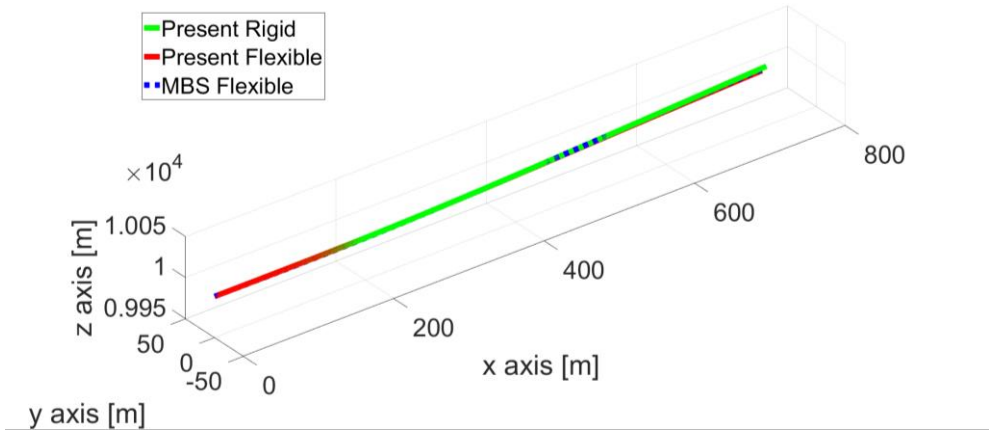

(a) flight path

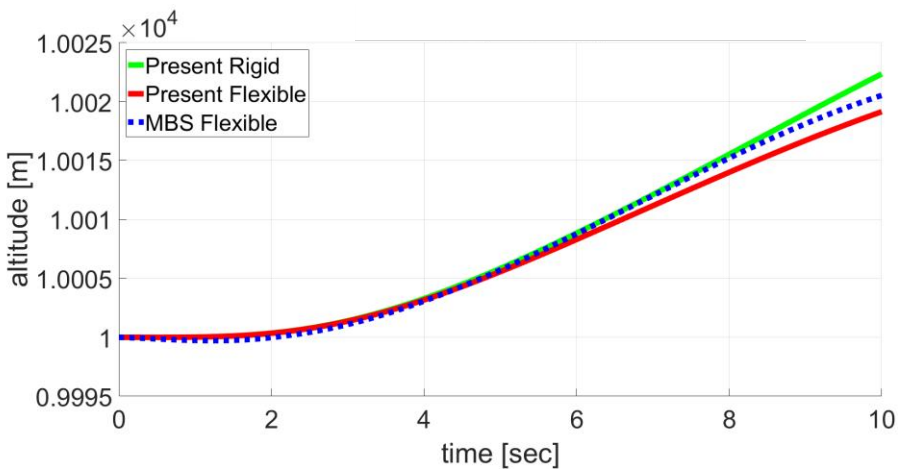

(b) altitude

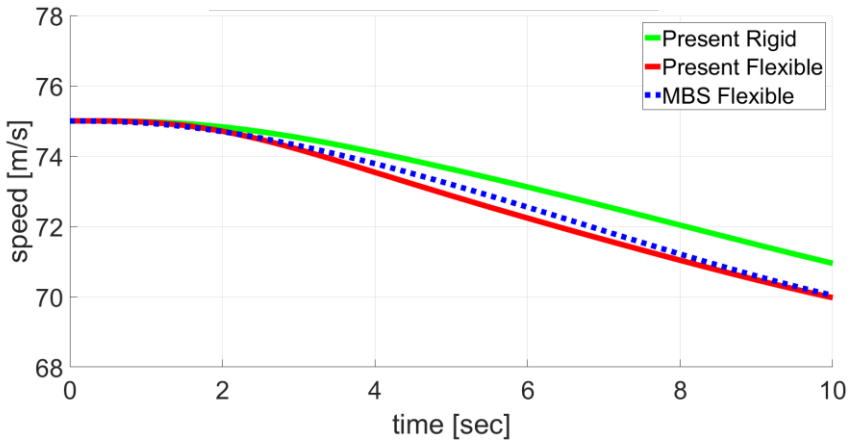

(c) true air speed

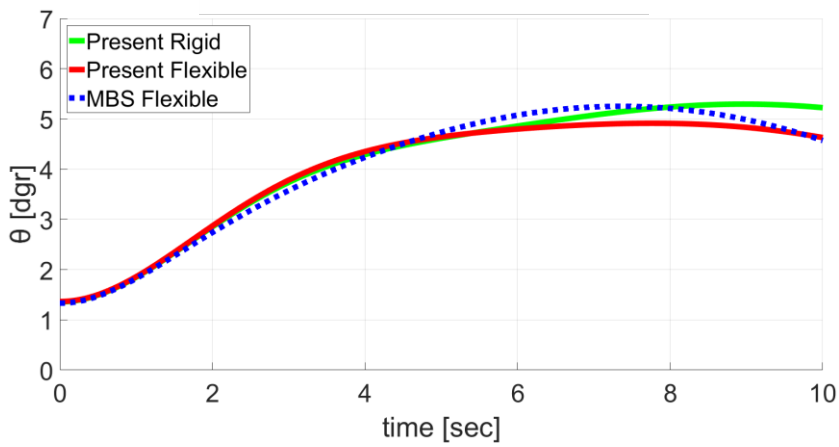

(d) Euler angle

Figure 3.5 Comparison of the pitch-up flight simulation

3.1.3 Simulation Results of Response to Aileron Control Input

The response of the aircraft under the operation an aileron was simulated. The simulation was carried out for a total duration of 10 seconds by prescribing the aileron control signal of (-) 0.5 ° while maintaining the trim values of the level cruise for the elevator and thrust. When the aileron was engaged, the aircraft would be examined regarding both longitudinal and lateral coupling flight performance because it would move simultaneously in both rolling and pitching directions. Also, the snapshot method was applied to the simulation to consider the flexibility of the aircraft.

Figure 3.6 shows the predicted flight path, the attitude expressed by the Euler angle, and the state represented by the true air speed. First of all, it was confirmed that the aircraft exhibited a maneuver flight which turned to the left and the altitude was decreased. And the discrepancies between rigid and flexible aircraft assumption were caused by considering the flexibility effect. The longitudinal distance traveled was 748.7 m in average, the altitude change was (-) 2.15 m in average, and the lateral distance was 35.3 m in average. When comparing the results with the multibody dynamics simulation, the overall trends were consistent but slightly different. These discrepancies were also considered to be caused by different assumptions applied to both simulations.

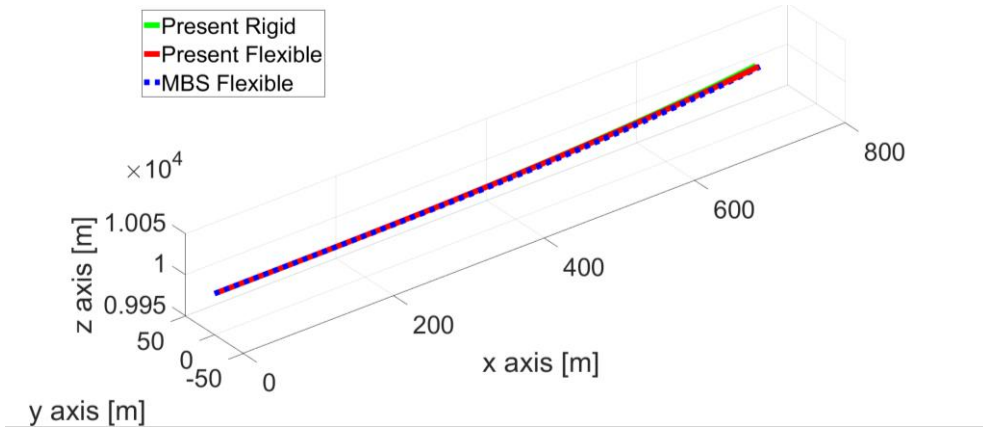

(a) flight path

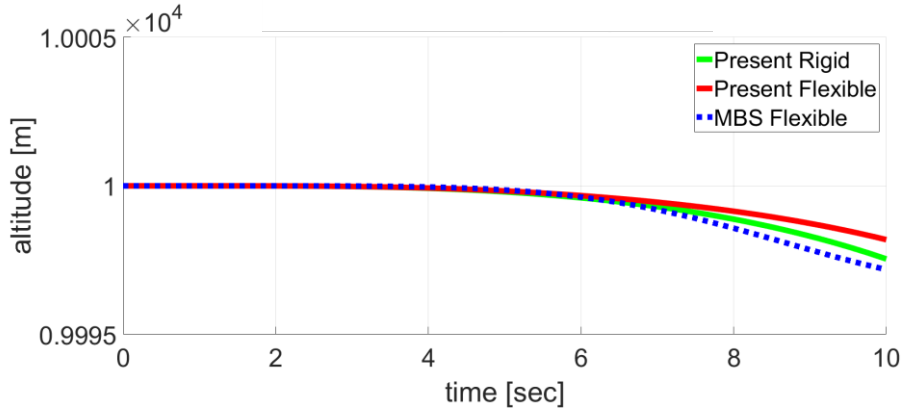

(b) altitude

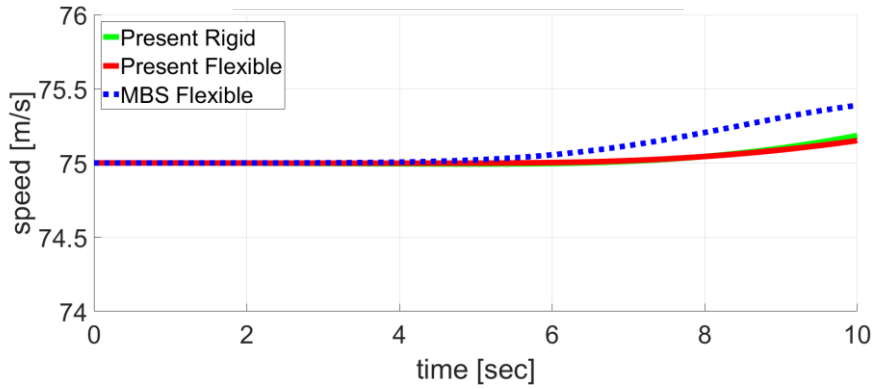

(c) true air speed

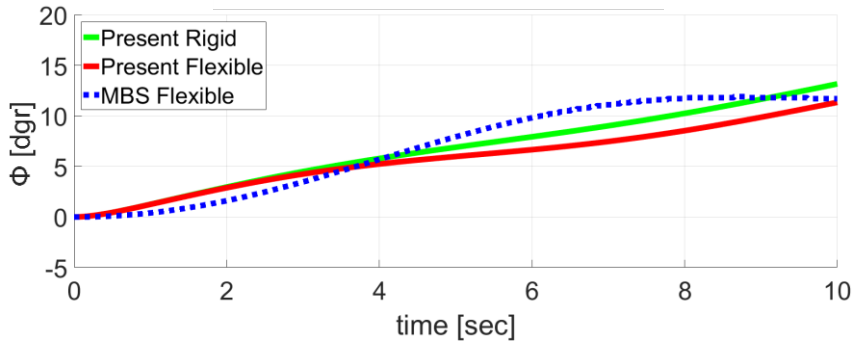

(d) Euler angle

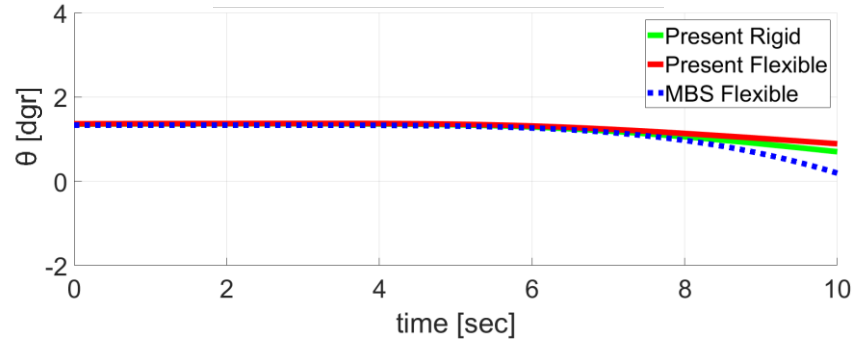

(e) Euler angle

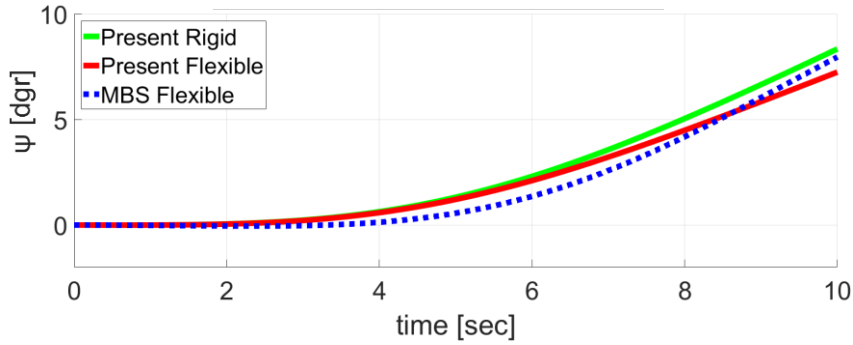

(f) Euler angle

Figure 3.6 Comparison of the left-turn flight simulation

3.2 Simulation of Response under Gust

3.2.1 Two-Dimensional Discrete Gust Profile

The effect of the gust that the aircraft encounters during flight causes an extreme change in aerodynamic forces acting on the wing, leading to a deformation of the wing structure. In this case, the aircraft generally changes its path and attitude due to the change of flight performance, or it causes damage to the structure in severe cases. Therefore, the simulation in predicting the response of the aircraft for the gust **e**ncounter to be prepared in advance is required [22]. In this thesis, a two-dimensional symmetric discrete gust of '1-cosine' profile was applied to the simulation as shown in Eq. (3.1). This gust module included in the MATLAB/Simulink program was used and the theoretical background was referred as specified in MIL-F-8785C [23].

$$V_{wind} = \begin{cases} 0 & x < 0 \\ \frac{V_m}{2}\left(1 - \cos\left(\frac{\pi x}{D_m}\right)\right) & 0 \le x \le D_m \\ V_m & x \ge D_m \end{cases} \tag{3.1}$$

The gust profile applied to the simulation was created by combining the two modules as shown in Table 3.4. At this time, the value was in accordance with Federal Aviation Regulations Part 25 Standards, and the gust would impinge in the (-) *z* axis direction with respect to the body fixed coordinate system. The flight altitude was 10,000 m and the speed was 75 m/s. Initial state of the aircraft was trimmed in the longitudinal level cruise.

Table 3.4 Profile and configuration of two-dimensional '1-cosine' discrete gust

Parameter	Value	Configuration
V_m	4.7 [m/s]	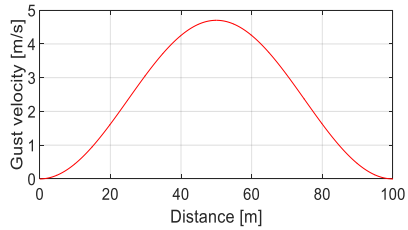
D_m	50 [m]	
x	0~100 [m]	

3.2.2 Simulation Results of Response under Gust

As shown in Figure 3.7, the altitude was abruptly increased while the aircraft passed the region of gust, and thereafter, it was confirmed that the flight was stable. At this time, discrepancy in flight path and attitude was obviously induced depending on the flexibility of the aircraft. Especially, in the section where the speed of the aircraft changed suddenly while passing through the gust region, the aircraft wing was deformed significantly and the aerodynamic performance was degraded. As a result, the attitude and path of the aircraft were changed. These effects were surely found to be more apparent in the gust **e**ncounter than in the soft and slow maneuver flight of the aircraft.

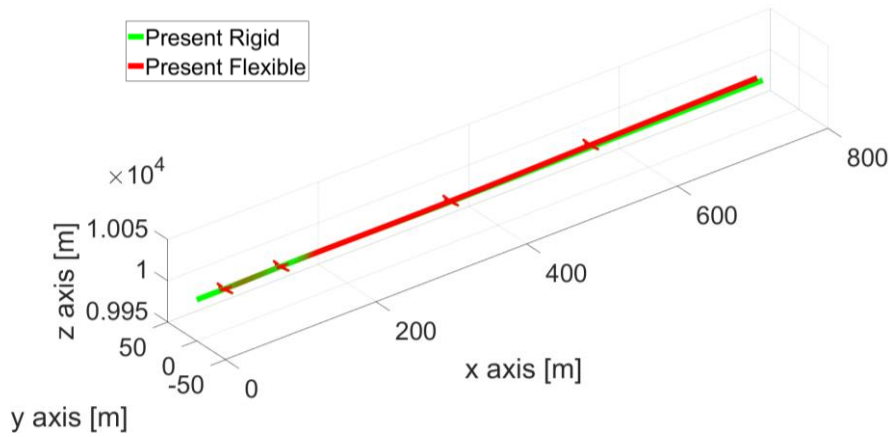

(a) flight path

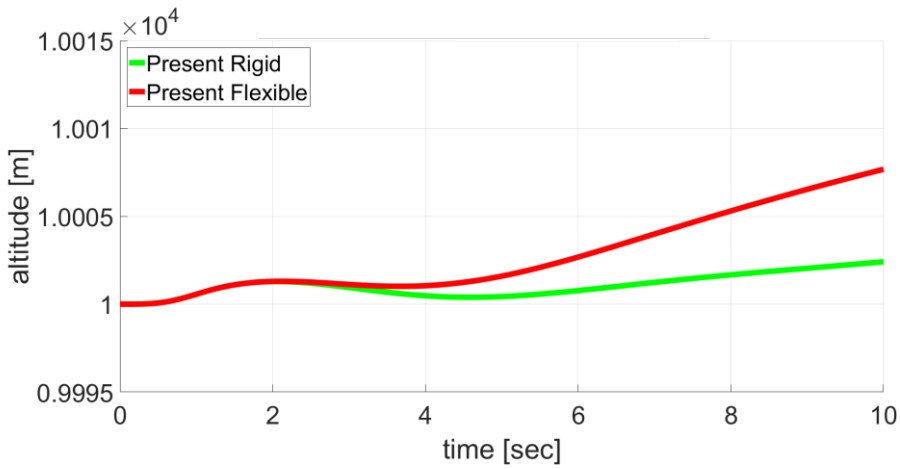

(b) altitude

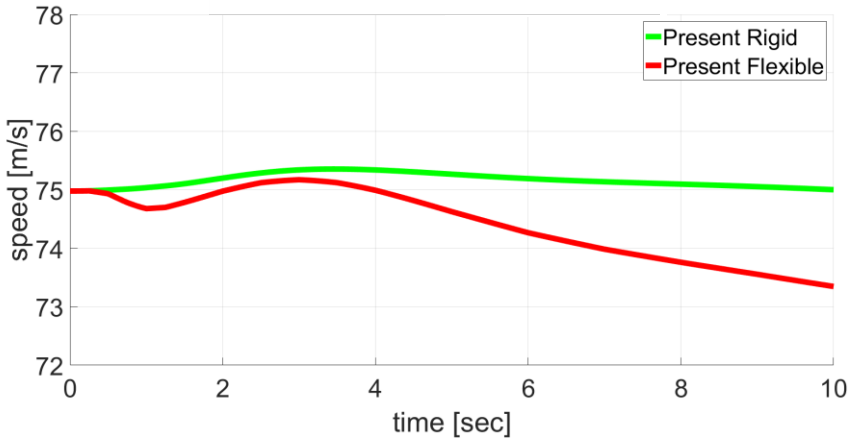

(c) true air speed

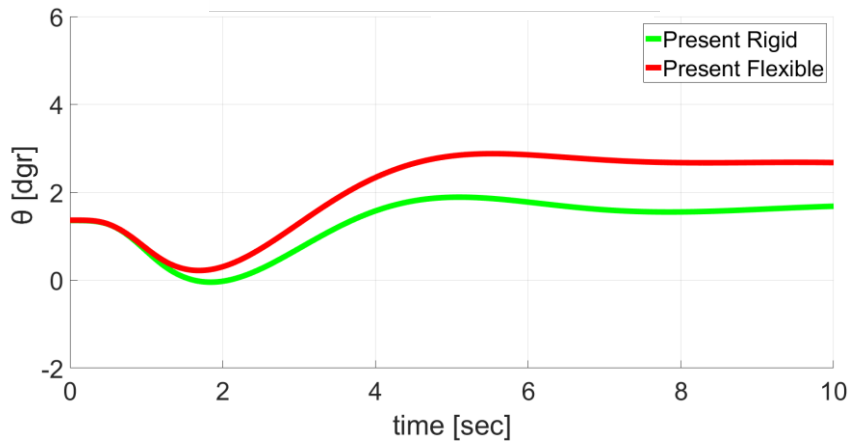

(d) Euler angle

Figure 3.7 Simulation results under the gust

3.2.3 Structural Deformation of UAV under Gust

From the results obtained by the simulation, the deformation amount of the aircraft from the structural model could be derived at each time step of iteration. From this result, the most extreme moments of the deformation were identified and the load and stress distribution information on the aircraft structure could be extracted. Figure 3.8 shows the flight path and the deformations of the UAV when the structural deformation was relatively large in the gust encounter. It was found that the deformation was large at the peaks of the speed. At this time, the deformation of the wing is shown in Figure 3.8 as a transition displacement at the wing tip. Displacement of the wing tip was about 0.1 m on the peak to peak, which was 20 % larger than the deformation for a cruise condition. This information is expected to be useful in the structural design of the aircraft during the development process.

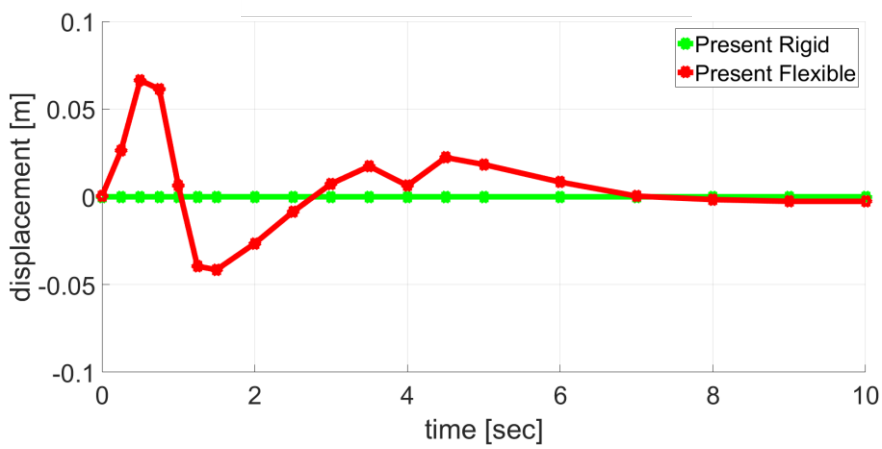

Figure 3.8 Wing tip deflection under the gust

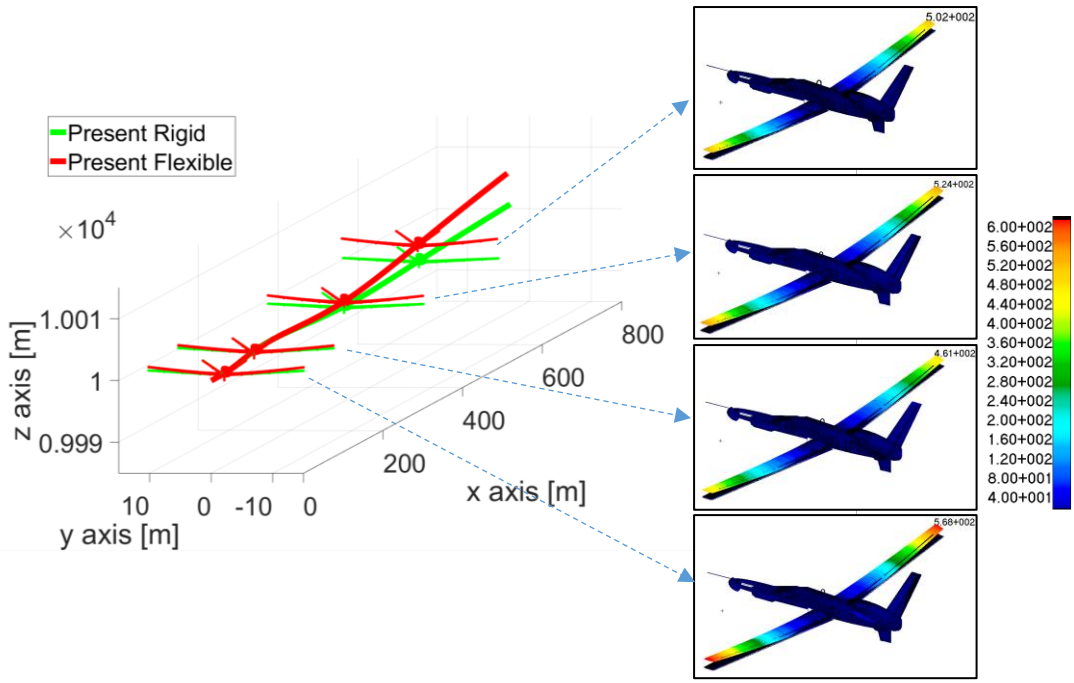

Figure 3.8 Flight paths and structural deformations of aircraft under the gust

IV. Conclusions

4.1 Summary

An improved methodology, snapshot method, has been suggested and developed to implement analysis with six degrees-of-freedom flight simulation that takes into account the flexibility of aircraft with high aspect ratio wings. This method is a temporal coupling scheme for sequential calls of different single-field solvers; for the flow field, for the structural deformation and for the rigid body motion. By repeated at discrete time step, the present coupled iterations represent instances of information exchange among the fields during the convergence towards the steady state.

MATLAB/Simulink analyzes the flight dynamics of the rigid motion and MSC.Flightload performs the quasi-steady aeroelastic trim analysis. Those elements were adopted as the solver of each field to establish the present simulation framework. A medium altitude unmanned aerial vehicle was analyzed by utilizing the present simulation framework. The simulation was performed under various conditions as follows and the conclusions were obtained.

1) Trim analysis for level cruise conditions were performed to determine the trim parameters required for the simulation operation. The determined trim parameters were compared with the other existing multibody dynamics simulation results and validated within average difference of 2.15 %.

Aerodynamic stability derivatives were estimated from aerodynamic model, and inertial moments were derived from structural model. Based on that information, the simulation of the level cruise state was performed and the results were compared with the simulation results of the existing multibody dynamics analysis.

2) In order to validate the present simulation, a pitch-up maneuver was examined by operating the elevator and a left-turn maneuver was by operating the ailerons of control surfaces. These results were compared with the other existing multibody dynamics simulation results and the longitudinal or lateral flight analysis performance of the simulator was verified. And the difference between the result for rigid and flexible aircraft assumptions was due to aerodynamic change due to structural deformation and degradation of flight performance caused by this effect.

3) Two-dimensional symmetric discrete gust profile of '1-cosine' shape was applied to the aircraft. Simulation was performed to predict the dynamic response of the aircraft passing through the gust region during flight. As a result, the flight attitude and path changed drastically, and the difference between the rigid and flexible aircraft assumptions became significant. Structural deformation was confirmed by displacement of the wing tip and the peak to peak value was about 0.1 m, which was 10 % larger than the

deformation for a cruise condition. This difference was due to increase of the effect of relatively large deformation of the structure compared to the soft and slow maneuver flight conditions. Therefore, information such as load, deformation, and stress distribution acting on the structure was extracted from the simulation results because it would be useful in designing the aircraft during the development process.

4.2 Future Works

There are a few challenging further works as follows.

For a short period, the present simulation will be supplemented to improve the accuracy and efficiency. First of all, the adoption of the presently improved analysis in each area enables a wider variety of nonlinear analysis. To the next the, three-dimensional asymmetric gust profile can be used to predict the dynamic response of the aircraft in a more complex gust. Then, the algorithm of the automatic flight control system used in the aircraft is required in the simulation to improve the accuracy to the level similar to the realistic flight environment.

For a long term, suggestion may be focused on a methodology that identifies both internal and external transient loads acting on aircraft structures during flight, by investigating improved simulation and flight test results in the reverse fashion.

References

[1] Drela, M., “Method for Simultaneous Wing Aerodynamic and Structural Load Prediction,” American Institute of Aeronautics and Astronautics, pp.322-332, 1989

[2] Brown, E., “Integrated Strain Actuation In Aircraft With Highly Flexible Composite Wings,” Ph.D Thesis, Massachusetts Institute of Technology, 2003

[3] Shearer, C., “Coupled Nonlinear Flight Dynamics, Aeroelasticity, and Control of Very Flexible Aircraft,” Ph.D Thesis, University of Michigan, 2006

[4] Su, W., “Coupled Nonlinear Aeroelasticity And Flight Dynamics of Fully Flexible Aircraft,” Ph.D Thesis, University of Michigan, 2008

[5] Collar, A. R., “The Expanding Domain of Aeroelasticity,” Royal Aeronautical Society Journal, Vol. 50, pp. 613~636, Aug. 1946

[6] Brewer, G., “The Collapse of Monoplane Wings,” Flight, January 1913

[7] Lanchester, F. W., “Torsional Vibrations of the Tail of an Airplane,” ARC Reports and Memoranda, No. 276, Part I, 1916

[8] Bryan, G. H., “Stability in Aviation,” Macmillan, 1911

[9] Etkin, B., Reid, L. D., “Dynamics of Flight - Stability and Control,” Wiley and Sons, 1996

[10] Bisplinghoff, R. L., Ashley H., Halfman, R. L., “Aeroelasticity,” Addison-Wesley, 1955

[11] Eggleston, J. M., Mathews, C. M., “Application of Several Methods for Determining Transfer Functions and Frequency Response of Aircraft from Flight Data,” Technical Note, National Advisory Committee for Aeronautics (NACA), NACA TN 2997, 1953

[12] Waszak, M. R., Schmidt, D. K., “Flight Dynamics of Aeroelastic Vehicles,” Journal of Aircraft, Vol. 25, No. 6, pp. 563-571, 1988

[13] Drela,M., “ASWING 5.81 Technical Description—Steady Formulation,” Technical Report, Massachusetts Institute of Technology, 2008

[14] Wellmer, G., “A Modular Method for the Direct Coupled Aeroelastic Simulation of Free-Flying Aircraft,” Ph.D Thesis, RWTH Aachen University, 2014

[15] Farhat, C., Pierson, K., Degand, C., “Multidisciplinary Simulation of the Maneuvering of an Aircraft,” Engineering with Computers, Vol. 17, pp. 16-27, 2001

[16] Schmidt, D. K., Raney, D. L., “Modeling and Simulation of Flexible Flight Vehicles,” JOURNAL OF GUIDANCE, CONTROL, AND DYNAMICS, Vol. 24, No. 3, 2001

[17] Spieck, M., Krüger, W., Arnold, J., “Multibody Simulation of the Free-Flying Elastic Aircraft,” American Institute of Aeronautics and Astronautics Conference, 2005

[18] Blakelock, J. H., “Automatic Control of Aircraft and Missiles,” A Wiley-Interscience publication, 2dn ed., USA, 1991

[19] Rodden, W. P., Love, J. R., “Equations of Motion of a Quasisteady Flight Vehicle Utilizing Restrained Static Aeroelastic Characteristics”, 25th Conference of American Institute of Aeronautics and Astronautics, 1985

[20] Bekey, G. A., Karplus, W. J., “Hybrid Computation,” John Wiley and Sons, New York, 1968

[21] “MSC/NASTRAN Aeroelastic Analysis User's Guide,” 68th Ed., MSC Software, Newport Beach in USA, 1994.

[22] Rodden, W. P., Revell, J. D., “The status of unsteady aerodynamic influence coefficients,” Inst. Aerospace Sci., Paper FF-33, January 1962.

[23] Nelson, R. C., “Flight Stability and Automatic Control,” WCB/McGraw-Hill, 2nd Edition, New York in USA, 1998

[24] Sikes G., Neill D. J., “MSC/Flight Loads and Dynamics”, MSC Software, Newport Beach in USA, 2001.

[25] Egle D., Ausman J., “INTEGRATION OF MSC.FLIGHTLOADS AND DYNAMICS AT LOCKHEED MARTIN AERONAUTICS COMPANY,” MSC Software, Newport beach in USA, 2001

[26] Kim, S., Chang, S., Jang, S., and Cho, M., “Flexible Aircraft Flight Dynamic Analysis with Discrete Gust,” KSAS 2016 Fall Conference, 2016

국문 초록

고세장비 날개를 가지는 항공기의 6 자유도 비행동역학 시뮬레이션을 위한 스냅샷 기법의 개발

빈 영 빈
기계항공공학부
서울대학교 대학원

본 연구에서는 3 차원 구조해석 모델을 활용하여 고세장비 날개를 가지는 항공기의 유연성이 고려된 6 자유도 비행 시뮬레이션 프로그램을 개발하였다. 주날개의 세장비가 20 이상이며 주로 높은 고도에서 장기 체공 비행을 하는 무인항공기(HALE)를 연구 대상으로 채택하였고 3 차원 전기체 유한요소 모델을 적용하였다. 이러한 항공기의 유연성을 고려하여 비행 중 동적 반응을 시간 영역에서 해석할 수 있도록 공기역학-탄성체 구조역학-비행역학을 결합한 'snapshot method'를 개발하였다. 이 기법을 적용하여 강체 운동을 예측하는 MATLAB/Simulink 와 공력탄성학 트림 해석을 담당하는 MSC.FlightLoads 가 긴밀하게 연결된 통합 시뮬레이션 프레임워크를 구축하였다.

기 개발된 시뮬레이터 사용하여 여러 기동 조건에서 따른 응답의 시뮬레이션을 수행하였다. 수평 비행에 대한 트림 해석을 수행하였고 그 결과로 트림 변수와 공기역학적 안정 미계수, 관성모멘트 등을 도출하였다. 이 정보를 바탕으로 러더베이터와 에일러론 등 조종면 작동에 따른 항공기 기동 비행의 시뮬레이션을 수행하였으며 강체와 유연 동체 가정에 의거한 효과를 확인하였다. 또한 동일한 조건을 적용한 다물체 동역학 기반의 시뮬레이션 결과와 비교 검증하였다. 그리고 돌풍에 대한 항공기의 응답을 예측할 수 있도록 시뮬레이션에 2 차원 1-cosine 이산화 돌풍 분포를 적용하여 시뮬레이션을 수행하였다.

주요어 : 고세장비 날개, 무인항공기, 6 자유도 비행 시뮬레이션, 유동-구조-강체운동 결합 해석, 비행동역학, 공력탄성학, MATLAB/Simulink, MSC.FlightLoads

학 번 : 2015-20775